学位論文

LSD1 mediates metabolic reprogramming
by glucocorticoids during myogenic differentiation
（骨格筋分化において、LSD1 酵素はグルココルチコイドによる代謝プログラムを調節する）

阿南　浩太郎

Kotaro Anan

指導教員

中　村　公　俊　教授
熊本大学大学院医学教育部博士課程医学専攻小児科学

中　尾　光　善　教授
熊本大学大学院医学教育部博士課程医学専攻細胞医学

２０１８年度

学　位　論　文

Doctoral Thesis

論文題名　：　LSD1 mediates metabolic reprogramming by glucocorticoids during myogenic differentiation

（骨格筋分化において、LSD1 酵素はグルココルチコイドによる代謝プログラムを調節する）

著 者 名　：　阿南　浩太郎
Kotaro Anan

指導教員名　：　熊本大学大学院医学教育部博士課程医学専攻小児科学　中村　公俊　教授
熊本大学大学院医学教育部博士課程医学専攻細胞医学　中尾　光善　教授

審査委員長：　病態生化学担当教授　山縣　和也

審査委員：　臨床病態解析学担当教授　松井　啓隆

幹細胞誘導学担当教授　江良　択実

分子生理学担当准教授　魏　范研

２０１８年度

Nucleic Acids Research, 2018 **1**
doi: 10.1093/nar/gky234

LSD1 mediates metabolic reprogramming by glucocorticoids during myogenic differentiation

Kotaro Anan[1,2], Shinjiro Hino[1,*], Noriaki Shimizu[3], Akihisa Sakamoto[1], Katsuya Nagaoka[1], Ryuta Takase[1], Kensaku Kohrogi[1,2], Hirotaka Araki[1], Yuko Hino[1], Shingo Usuki[4], Shinya Oki[5], Hirotoshi Tanaka[3], Kimitoshi Nakamura[2], Fumio Endo[2] and Mitsuyoshi Nakao[1,*]

[1]Department of Medical Cell Biology, Institute of Molecular Embryology and Genetics, Kumamoto University, Kumamoto 860-0811, Japan, [2]Department of Pediatrics, Graduate School of Medical Sciences, Kumamoto University, Kumamoto 860-0811, Japan, [3]Division of Rheumatology, Center for Antibody and Vaccine Therapy, IMSUT Hospital, The Institute of Medical Science, The University of Tokyo, Tokyo 108-8639, Japan, [4]Liaison Laboratory Research Promotion Center, Institute of Molecular Embryology and Genetics, Kumamoto University, Kumamoto 860-0811, Japan and [5]Department of Developmental Biology, Graduate school of Medical Sciences, Kyushu University, Fukuoka 812-8582, Japan

Received February 14, 2018; Revised March 15, 2018; Editorial Decision March 16, 2018; Accepted March 20, 2018

ABSTRACT

The metabolic properties of cells are formed under the influence of environmental factors such as nutrients and hormones. Although such a metabolic program is likely initiated through epigenetic mechanisms, the direct links between metabolic cues and activities of chromatin modifiers remain largely unknown. In this study, we show that lysine-specific demethylase-1 (LSD1) controls the metabolic program in myogenic differentiation, under the action of catabolic hormone, glucocorticoids. By using transcriptomic and epigenomic approaches, we revealed that LSD1 bound to oxidative metabolism and slow-twitch myosin genes, and repressed their expression. Consistent with this, loss of LSD1 activity during differentiation enhanced the oxidative capacity of myotubes. By testing the effects of various hormones, we found that LSD1 levels were decreased by treatment with the glucocorticoid dexamethasone (Dex) in cultured myoblasts and in skeletal muscle from mice. Mechanistically, glucocorticoid signaling induced expression of a ubiquitin E3 ligase, JADE-2, which was responsible for proteasomal degradation of LSD1. Consequently, in differentiating myoblasts, chemical inhibition of LSD1, in combination with Dex treatment, synergistically de-repressed oxidative metabolism genes, concomitant with increased histone H3 lysine 4 methylation at these loci. These findings demonstrated that LSD1 serves as an epigenetic regulator linking glucocorticoid action to metabolic programming during myogenic differentiation.

INTRODUCTION

Environmental factors exert profound influences on the epigenome, leading to phenotypic variations in cells and organisms (1). In particular, nutritional conditions, such as malnutrition and high fat feeding, induce genome-scale rearrangement of epigenomic signatures, including DNA methylation and histone modifications (2,3). However, direct mechanistic links between environmental cues and the activities of individual chromatin modifiers are poorly understood.

Lysine-specific demethylase-1 (LSD1 or KDM1A) is a member of the amine oxidase family that catalyzes demethylation of methylated lysine side chains within proteins, including histone H3 lysine 4 (H3K4) (4,5). LSD1 contributes to a variety of cellular processes, such as stem cell maintenance, development and carcinogenesis (6–8). We previously demonstrated that LSD1 epigenetically suppressed oxidative phosphorylation (OXPHOS) through H3K4 demethylation in adipogenic and cancer cells (9,10). Notably, metabolic regulation by LSD1 depended on environmental conditions such as energetic state, hormones and neurological stimuli (9,11), indicating that LSD1 reacts to the nutritional and metabolic conditions of cells and modulates their metabolic properties.

*To whom correspondence should be addressed. Tel: +81 96 373 6800; Fax: +81 96 373 6804; Email: s-hino@kumamoto-u.ac.jp
Correspondence may also be addressed to Mitsuyoshi Nakao. Email: mitnakao@kumamoto-u.ac.jp

In mammals, skeletal muscle is composed of mechanically distinct fiber types, each having unique metabolic properties (12). Slow-twitch (type I) fibers participate in persistent mechanical activities, such as posture, through their slow contractile activity, supported by a high capacity for OXPHOS. In contrast, fast-twitch (type II) fibers, with their shift toward anaerobic energy production, are capable of fast contraction, contributing to strong and dynamic movements. Skeletal muscle can flexibly alter its metabolic character in response to environmental factors, contributing to energy homeostasis and physical fitness. Anabolic hormones, such as insulin, activate the glycolytic program under nutritionally rich conditions. On the other hand, when energy sources are scarce, catabolic hormones, such as glucocorticoids, activate oxidative metabolism and suppress formation of the fast fibers (13). Previous studies established that dynamic epigenomic remodeling, including histone modifications and DNA methylation, contribute to highly ordered expression of myogenesis-associated genes (14,15). However, it is unknown how these environmental contexts can be translated into epigenetic remodeling in myogenic cells.

In this study, we demonstrated that LSD1 directly repressed expression of oxidative metabolism and slow myosin genes in differentiating myoblasts, resulting in enhanced OXPHOS capacity in myotubes. We also found that glucocorticoid signaling induced expression of an E3 ligase, JADE-2, leading to proteasomal degradation of LSD1. LSD1 inhibition, in combination with Dex treatment, significantly increased expression of oxidative genes and H3K4 methylation levels, indicating that LSD1 counteracted the glucocorticoid-mediated gene regulation. Our study demonstrated a novel epigenetic mechanism linking hormonal signaling to metabolic reprogramming during myogenic differentiation.

MATERIALS AND METHODS

Cell culture

C2C12 mouse myoblasts and Hepa1-6 mouse hepatoma cells were maintained in Dulbecco's Modified Eagle's Medium (DMEM, Sigma-Aldrich) supplemented with 10% (v/v) heat-inactivated fetal bovine serum (FBS) in a 37°C incubator equilibrated with 95% air, 5% CO_2. For myogenic induction, subconfluent C2C12 myoblasts were cultured in DMEM with 2% (v/v) horse serum. The medium was changed every other day. For protein assays, Hepa1-6 cells were cultured for 48 h in DMEM supplemented with 10% (v/v) dextran-coated charcoal (DCC)-treated FBS followed by treatment with 1 μM dexamethasone (Sigma-Aldrich) for 48 h. For immunofluorescence, Hepa1-6 cells were cultured for 24 h in DMEM supplemented with 2% (v/v) DCC-treated FBS followed by treatment with 1 μM Dex for 24 h.

For shRNA expression, SureSilencing Plasmids harboring shRNA against LSD1 (shLSD1, #336312 KM27305H, Qiagen) and non-targeting control (shControl, Qiagen #336312) were used. C2C12 cells were transfected with shLSD1 and shControl vectors using FuGENE6 Transfection Reagent (Promega). Stable transfectants were selected in the presence of 750 μg/ml hygromycin B (Wako). For transient siRNA introduction, specific siRNAs were introduced to the Hepa1-6 cells using RNAiMAX reagent (Invitrogen) when they were ∼50% confluent. The effective siRNA target sequences are as follows: siGL3 (control) CTTACGCTGAGTACTTCGA, siJade2 CGTTAG AGCGTGTTCTAGA.

Reagents and antibodies

Tranylcypromine hydrochloride, dexamethasone, insulin (bovine pancreas), testosterone, 3,3′,5-triiodo-L-thyronine, MG132 and cycloheximide were from Sigma-Aldrich. S2101 was from Millipore. 17-β-Estradiol was from Wako. The antibodies used were anti-LSD1 (Abcam, ab17721), anti-mono-methylated histone H3K4 (Abcam, ab8895), anti-di-methylated histone H3K4 (Millipore, 07-030), anti-tri-methylated histone H3K4 (Millipore, 07-473), anti-pan histone H3 (Abcam, ab1791), anti-myosin heavy chain (Santa Cruz, sc-20641), anti-slow-myosin (Sigma-Aldrich, M8421), anti-glucocorticoid receptor (Santa Cruz, sc-8992) and anti-PHF15 (JADE-2) (Sigma-Aldrich, HPA025959).

Animal studies

Animal experiments were conducted in accordance with the guidelines of the Animal Care and Use Committee of Kumamoto University and the Animal Ethics Committee of the Institute of Medical Science, The University of Tokyo. For gene expression analysis in gastrocnemius and soleus muscle, 8-week-old male C57BL/6J mice were fasted for 4 h, then sacrificed. Intraperitoneal (i.p.) administration of dexamethasone (Dex) to mice harboring skeletal muscle-specific deletion of glucocorticoid receptor (GRmKO) was performed as previously described (16). Briefly, 11-week-old male $GR^{flox/flox}$ (control) and GRmKO mice were injected with Dex at 1 mg/kg or vehicle (saline), daily for 7 days, then were sacrificed. Adrenalectomy was performed as previously described (16). Briefly, 19-week-old male C57BL/6J mice were adrenalectomized and maintained with 0.9% sodium chloride in the drinking water for 7 days, then sacrificed.

Myoblast isolation and culture

Mouse myoblasts were isolated as described previously with some modifications (17). Briefly, hindlimbs of 2-day-old C57BL/6J mice were removed and muscle was separated from the skin and bone with sterile forceps. The cells were dispersed with 0.2% collagenase I (Gibco) and 0.2% Dispase II (Sigma-Aldrich) for 30 min, and then filtered through a 40 μm cell strainer. To remove non-myogenic cells, cells were plated on normal culture dish and incubated for 30 min. Subsequently, floating cells were re-plated on a collagen coated culture dish. Myoblasts were initially cultured in Ham's F10 nutrient mixture (Gibco) and then the medium was switched to DMEM/Ham's F10 (1:1). Both growth media were supplemented with 20% FBS, 2.5 ng/ml bFGF and 1% penicillin/streptomycin. To induce differentiation, myoblasts were cultured in DMEM with 5% HS and penicillin/streptomycin. Medium was changed every other day.

Quantitative RT-PCR

Total RNA from cells was extracted using a Trizol reagent (Invitrogen). Complementary DNA was synthesized using a ReverTra Ace qPCR RT Kit (Toyobo). Quantitative real-time PCR was performed using THUNDERBIRD SYBR qPCR Mix (Toyobo) and an ABI 7300 Real-Time PCR System (Applied Biosciences). Relative RNA quantities were calculated by ΔΔCt method. Primers are listed in Supplementary Table S1.

Microarray analysis

Genome-wide expression analysis was performed using a GeneChip Mouse Genome 430 2.0 Array in combination with a GeneChip Hybridization, Wash and Stain Kit (Affymetrix). TC- and S2101-treated or shLSD1 stably expressing C2C12 cells were induced to differentiate for 48 h, followed by RNA extraction and a quality check using a Bioanalyzer RNA 6000 Nano Assay (Agilent). Data annotation analysis was performed using GeneSpring GX software (Agilent). Gene set enrichment analysis was performed using GSEA version 2.0 from the Broad Institute of MIT and Harvard (Cambridge, MA, http://www.broadinstitute.org/gsea/). Significantly enriched gene sets were identified by using the criterion of nominal P-value < 0.05 and FDR q-value < 0.25 according the software instructions (http://software.broadinstitute.org/gsea/index.jsp).

Chromatin immunoprecipitation (ChIP)

ChIP experiments for detecting modified histones and glucocorticoid receptor were performed as previously described (10). Briefly, cells were crosslinked with 1% formaldehyde, then sonicated for chromatin fragmentation. ChIP experiments for detecting LSD1 enrichment were performed according to the Epigenesys protocol by Porro and Perini (Prot 29, http://www.epigenesys.eu/), with some modifications. Briefly, dual crosslinking using 1% formaldehyde and disuccinimidyl glutarate (DSG) (ThermoFisher Scientific) was performed to increase stability of protein-DNA complexes. All chromatin fragmentation was done in a RIPA buffer (50 mM Tris–HCl, 150 mM NaCl, 2 mM EDTA, 1% NP-40, 0.1% SDS and 0.5% sodium deoxycholate) by two-step sonication, first with a probe-type sonifier (Branson) and then with a water bath sonifier, Bioruptor (Cosmo Bio). Chromatin fragments were incubated at 4°C overnight with the appropriate antibodies, followed by a pulldown using protein A/G-conjugated agarose beads (Millipore) or Dynabeads protein A/G (Life Technologies). Purified DNA was subjected to quantitative PCR (qPCR).

ChIP-seq analysis

For ChIP-seq analyses to detect LSD1–DNA interactions, 5×10^7 C2C12 cells, differentiated for 2 days or 5 days, were collected. For analyses to detect methylated H3K4, 6.4×10^6 C2C12 cells, differentiated for 48 h with or without S2101, were collected. Crosslinking, fragmentation and immunoprecipitation were performed as described for ChIP. Each protein-bound chromatin fraction was collected using Dynabeads protein A/G (Life Technologies) and DNA was purified using an Agencourt AMPure XP (Beckman Coulter). A DNA fragment library for sequencing was constructed using NEBNext Ultra II DNA Library Prep Kit for Illumina (New England BioLabs). Adapter-ligated DNA fragments were purified using Agencourt AMPure XP. High-throughput sequencing was performed using a NextSeq 500 Desktop Sequencer (Illumina) according to the manufacturer's instructions. The qualified reads were aligned onto the mouse reference genome mm9 using the Bowtie 2 algorithm (18). Duplicate reads and reads with low overall quality or low mapping quality were excluded. The final numbers of mapped reads are listed in Supplementary Table S2. We identified 44,039 in day 2 and 17,446 in day 5 LSD1-enriched peaks across the whole genome using a model-based analysis of ChIP-Seq data (MACS) algorithm (19). LSD1 binding sites were detected based on the LSD1 peaks significantly enriched over input peaks at a P-cutoff value of 10^{-5}. Detected LSD1 peaks were linked to neighboring genes with ChIPpeakAnno algorithm, measuring the distance from the TSS. The ChIP-seq data for Rest (GSM915175), Max (GSM915174), Six4 (GSM1633919), MyoD (GSM915165), and myogenin (GSM915164) were imported from the National Center for Biotechnology Information (NCBI). Data visualizations were performed with Strand NGS software (Strand Genomics). The prediction of co-occupancy of LSD1 with other proteins was done using ChIP-Atlas (http://chip-atlas.org/). Subsequent data analyses were performed on the Galaxy platform (http://usegalaxy.org/). The number of reads in LSD1 and pan- or modified-histone data were normalized to that of input data with the bamCompare tool. Enrichment values of LSD1 around histone modifications or Pol II peaks were calculated with the computeMatrix tool and visualized with the plotHeatmap tool. Our ChIP-seq data (H3K4me1, H3K4me2 and H3K4me3 in control cells) or the ones obtained from ChIP-Atlas with Q-value of 1.0×10^{-10} (pol II: SRX062103, H3K9me3: SRX862738 and H3K27ac: SRX103218) were used as references. Enrichment values of LSD1 and modified histones at LSD1 peaks were calculated with the multiBigwig tool.

Immunofluorescence and quantitative analysis

Cells were fixed with 4% paraformaldehyde in phosphate buffered saline (PBS) for 15 min at room temperature. The cells were washed 3 times with PBS for 5 min, then permeabilized with PBS containing 0.5% Triton X-100 for 5 min on ice. The cells were washed 3 times with PBS for 5 min then incubated with the primary antibodies for 60 min, followed by the Alexa 488-conjugated secondary antibody for 60 min. The cells were washed with PBS 3 times for 5 min each, after each incubation. DNA was counterstained with 1 μg/ml 5,6-diamidino-2-phenylindole (DAPI).

Quantitative analysis was performed with HCS Studio Analysis Software (ThermoFisher Scientific). To count nuclei in MHC-expressing myotubes, we used the 'Colocalization' command in the 'Bioapplication' tool of the HCS software. First, we identified a DAPI-stained nucleus as the main object, then defined regions of interest (ROIs) as

2-pixel rings around each nucleus. When an ROI was co-localized with the fluorescent signal of MHC, the nucleus was identified as an MHC-expressing nucleus. To quantify the area and intensity of the MHC signal, we used the 'Spot Detector' command in the 'Bioapplication' tool in HCS software, in which MHC-stained myofibers were identified as pixels with MHC signals.

Real-time measurement of OXPHOS activity

Real-time monitoring of cellular OXPHOS activity was performed using the XF24 Extracellular Flux Analyzer (Seahorse Bioscience), according to the manufacturer's instructions. C2C12 cells were seeded on the Seahorse assay plate and allowed to differentiate under LSD1 inhibition for 5 days before the assay. Maximum OXPHOS capacity was determined as previously described (9).

Determination of intracellular ATP

To determine intracellular ATP concentrations, C2C12 cells were allowed to differentiate under LSD1 inhibition for 4 days. After differentiation, cells were incubated in glucose-free DMEM (Gibco) with 1 mM sodium pyruvate and 2% HS for 3 h, and then, in the presence of 1g/l glucose for 15 min. Cells were collected and ATP concentrations were determined with an ATP Bioluminescence Assay Kit CLS II (Roche), according to the manufacturer's instructions. ATP concentration values were normalized to DNA contents, measured in the same samples.

Statistical analyses

Data are presented as means ± standard deviation (s.d.). All statistical analyses, except for microarray analyses, were performed to compare two groups. We first used F-test for examining equality of variances. Where variances were equal, two-tailed Student's *t*-test was used, and if not, two-tailed Welch's *t*-test was used. For microarray analyses, Pearson's χ^2 test was used.

RESULTS

LSD1 inhibition de-represses oxidative metabolism genes in differentiating myoblasts

To examine the role of LSD1 in transcriptional regulation during myogenesis, we treated differentiating C2C12 myoblasts with the enzymatic LSD1 inhibitors tranylcypromine (TC) or S2101 (Supplementary Figure S1A). TC is the first reported potent inhibitor of LSD1 (20), and S2101 is highly selective against LSD1 over structurally related enzymes including monoamine oxidases and LSD2 (21,22). Under our experimental conditions, LSD1 inhibition did not interfere with differentiation, as assessed by expression of myogenic markers, *Myod1* and *Myog*, and by myotube formation (days 5 to 7) (Supplementary Figure S1B–D) (23). We performed microarray-based expression analysis of differentiating C2C12 cells under LSD1 inhibition (day 2). We identified 253 genes whose signal intensities were increased by 1.5-fold or more in cells treated with TC and S2101 (Figure 1A). To test whether co-regulated genes were involved in specific biological processes, we performed a Gene Set Enrichment Analysis (GSEA) (24). GSEA identified 14 gene categories that were significantly upregulated by LSD1 inhibition, many of which were related to lipid and oxidative metabolism (Figure 1B and Supplementary Figure S2A). Conversely, gene categories such as 'cell cycle' and 'DNA replication' were downregulated by LSD1 inhibition (Supplementary Figure S2B). After differentiation (day 7), LSD1-inhibited cells maintained elevated expression of oxidative metabolism genes, compared with in controls (Figure 1C) (25). Because C2C12 myoblasts undergo fast twitch-like skeletal myogenesis upon induction (26), we next tested whether muscle structural genes were co-regulated with metabolic genes. We found that expression of slow fiber-associated genes, *myosin heavy chain-7* (*Myh7*) and *light chain-2* (*Myl2*), was significantly upregulated 2- to 3-fold in LSD1-inhibited myotubes (day 7), while that of fast-twitch genes, *Myh4*, *Myl1* and *Mylpf*, was less affected (Figure 1D). To further validate the effects of LSD1 inhibition on metabolic gene expression, we characterized the metabolic phenotype of myotubes formed under LSD1 inhibition. Maximum OXPHOS capacity of the cells was enhanced by LSD1 inhibition, while glycolytic activity was unaffected (Figure 1E, Supplementary Figure S3A and B). In addition, while intracellular ATP levels were decreased by glucose deprivation in control myotubes, LSD1-inhibited cells maintained constant ATP levels under glucose deprivation, indicating that LSD1 inhibition augmented OXPHOS-dependent energy production by using alternative fuels such as fatty acids (Figure 1F). We previously reported that LSD1 promoted expression of glycolytic genes through stabilization of HIF-1α protein in human hepatocellular carcinoma cells (10). In C2C12 myoblasts, glycolytic genes were mostly unaffected by LSD1 inhibition (Supplementary Figure S3C). These results show that inhibition of LSD1 demethylase activity during myogenesis activates oxidative metabolism in the resulting myotubes.

LSD1 is associated with transcriptionally competent chromatin

To identify LSD1-bound genes, we performed ChIP-seq analyses in differentiating (day 2) and differentiated (day 5) C2C12 cells. The number of LSD1-bound genes declined from 16,858 at day 2 to 9938 at day 5, of which 9613 were maintained throughout differentiation (Figure 2A). Substantial fraction of LSD1- bound regions was found within ±10 kb of the TSS (Figure 2B). To characterize the chromatin signature associated with LSD1 binding, we merged our LSD1-ChIP-seq results with publicly available ChIP-seq data from C2C12 cells. LSD1-bound sites prominently coincided with active chromatin marks, such as H3K4 methylation and H3K27 acetylation, but not with a repressive mark, H3K9me3 (Figure 2C, Supplementary Figure S4A and B). Furthermore, LSD1-bound regions were also coincident with RNA polymerase II (pol II), suggesting that LSD1 was enriched at transcriptionally competent chromatin. To identify transcription factors (TFs) and/or chromatin modifiers exhibiting distributions similar to that of LSD1, we compared our ChIP-seq data with published datasets using ChIP-Atlas (http://chip-atlas.org/). LSD1-

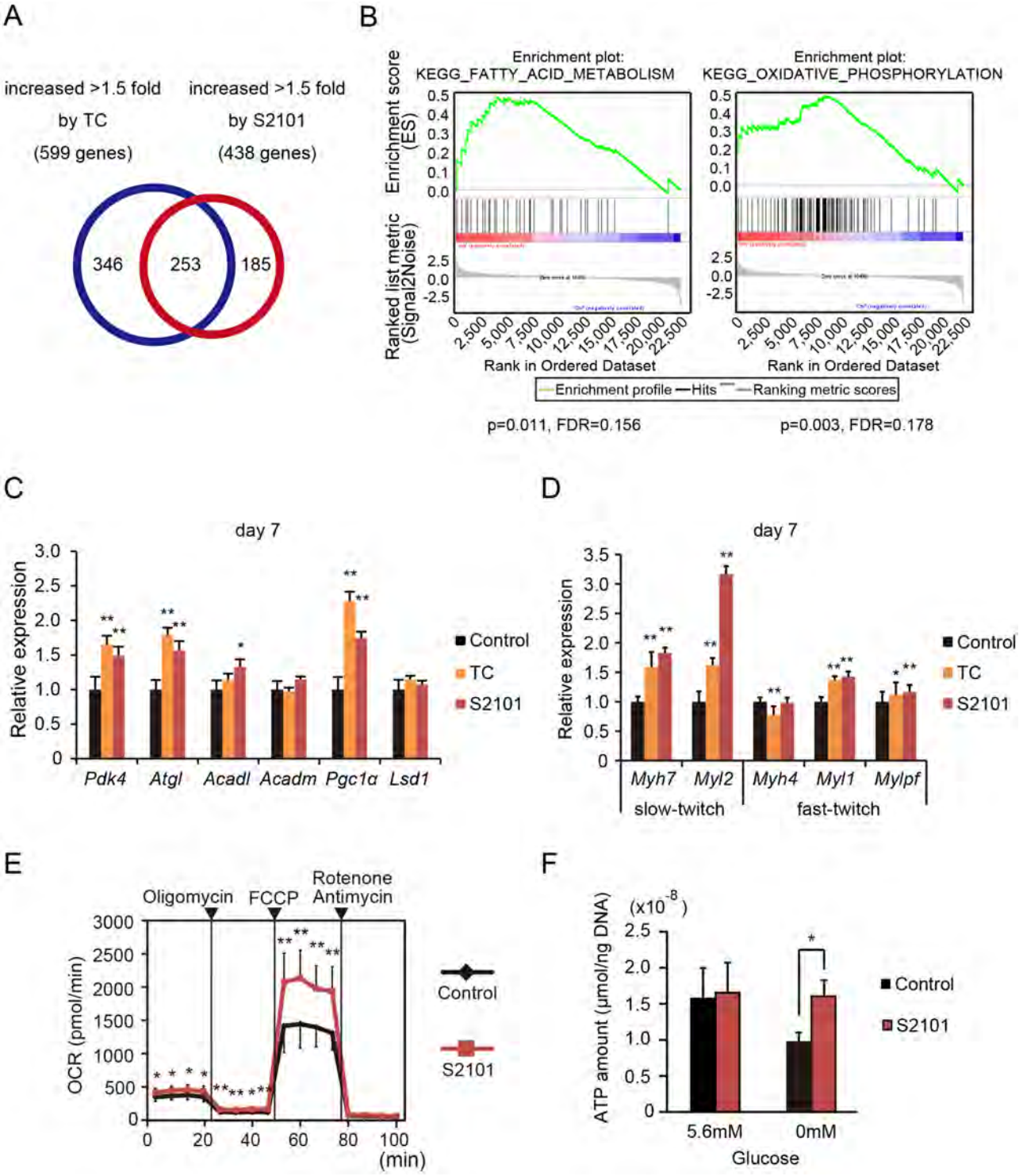

Figure 1. LSD1 inhibition during myogenic differentiation enhances expression of oxidative metabolism genes. (**A**) Venn diagram of genes increased more than 1.5-fold by treatment with LSD1 inhibitors, TC (10^{-4} M) or S2101 (10^{-5} M). C2C12 cells were analyzed at 48 h after myogenic induction. Vehicle was administered to the control samples. (**B**) Gene set enrichment analysis (GSEA) of genes upregulated by LSD1 inhibition. Nominal *p* values and false discovery rates (FDRs) are indicated. (**C** and **D**) Expression levels of LSD1 target genes (C) and slow and fast muscle myosin genes (D) in TC and S2101 treated cells ($n = 4$). Cells were cultured in differentiation medium for 7 days in the presence of LSD1 inhibitors. qRT-PCR values were normalized to values for the *36B4* gene and are shown as fold differences compared with vehicle-treated controls. Full names of the genes examined are listed in Supplementary Table S1. (**E**) Effects of LSD1 inhibition on the OXPHOS capacity of differentiated C2C12 cells. Oxygen consumption rate (OCR) is shown ($n = 10$). During real-time measurements, respiratory chain inhibitors were added to the medium at the indicated time points. Maximum OXPHOS capacity was evaluated as the maximized OCR levels under FCCP treatment. Values are means ± s.d. (**F**) Effects of LSD1 inhibition on glucose dependent ATP production. Intracellular ATP concentrations in differentiated cells in the presence or absence of glucose ($n = 3$). ATP concentration was normalized to DNA content. Detailed procedures are described in MATERIALS AND METHODS. $^{*}P < 0.05$, $^{**}P < 0.01$.

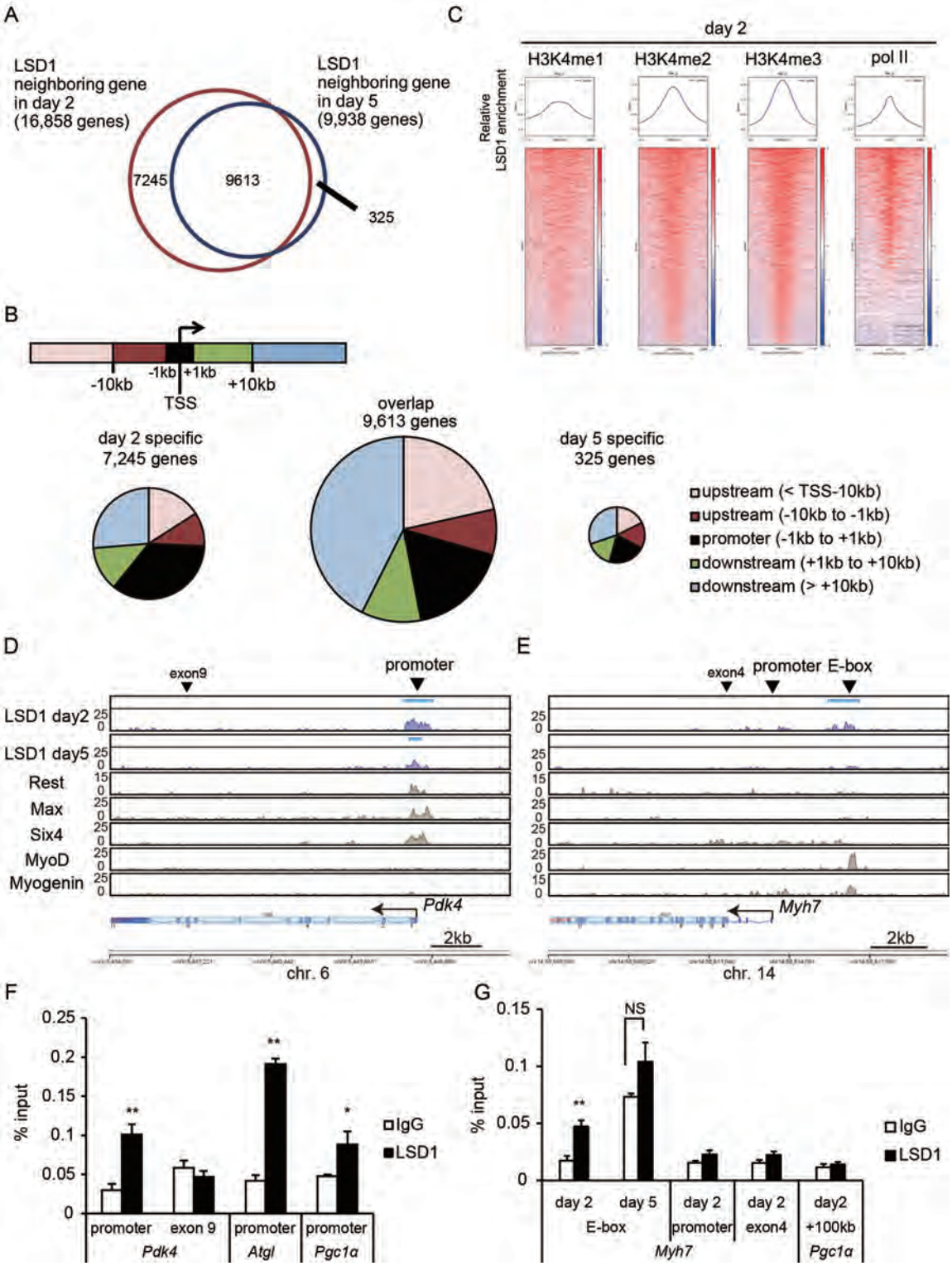

Figure 2. LSD1 is enriched at transcriptionally competent chromatin in differentiating myoblasts. (**A**) Venn diagram of LSD1 neighboring genes in differentiating (day 2) and differentiated (day 5) C2C12 cells. (**B**) Pie charts showing genomic distribution of LSD1 peaks. The regions were classified into five classes based on the distance from transcription starting site (TSS) of each neighboring gene. (**C**) LSD1 enrichment relative to methylated H3K4 and RNA polymerase II at day 2. Normalized enrichment values of LSD1 from –2 kb to +2 kb of indicated protein peaks are shown. (**D** and **E**) Enrichment of LSD1 at the *Pdk4* (D) and slow-associated *Myh7* (E) gene loci. Y axis indicates the read counts for each data. MACS LSD1 peaks are indicated by blue bars above the enrichment data. Data were visualized using Strand NGS software (Strand Genomics). Publicly available ChIP-seq data for Rest, Max, Six4, MyoD and myogenin in C2C12 cells are also shown (Data IDs are listed in MATERIALS AND METHODS). Arrowheads indicate the target regions for ChIP-qPCR. (**F** and **G**) ChIP-qPCR analyses of LSD1 occupancy at metabolic gene promoters (F) and *Myh7* gene loci (G). ChIP analyses were performed using differentiating (day 2) and differentiated (day 5) C2C12 cells ($n = 3$). $^{*}P < 0.05$, $^{**}P < 0.01$. NS: no significant difference.

Table 1. (**A** and **B**) Transcription factors (TFs) exhibiting similar genomic distributions to that of LSD1. LSD1 peaks were divided into two groups, LSD1-bound promoters (<TSS ± 1 kb) (A) and outside of promoters (>TSS ± 1 kb) (B). An extensive comparison with publicly available datasets was conducted for each group, using the ChIP-Atlas (http://chip-atlas.org/). Top 10 rankings are shown

Rank	ID	Antigen	Cell	Num of peaks	Overlaps / LSD1	Overlaps / random	Fold enrichment	*P*-value	*Q*-value
(A) TFs similarly distributed with LSD1 (<TSS ± 1 kb)									
1	SRX3206550	Brd4	Muscle, Skeletal	5236	4424/11268	27/11268	163.852	$<1.0 \times 10^{-324}$	$<1.0 \times 10^{-324}$
2	SRX3206547	Brd4	Muscle, Skeletal	6926	5690/11268	39/11268	145.897	$<1.0 \times 10^{-324}$	$<1.0 \times 10^{-324}$
3	SRX3206545	Brd4	Muscle, Skeletal	9561	7152/11268	50/11268	143.04	$<1.0 \times 10^{-324}$	$<1.0 \times 10^{-324}$
4	SRX142538	E2f4	C2C12	2379	1628/11268	13/11268	125.231	$<1.0 \times 10^{-324}$	$<1.0 \times 10^{-324}$
5	SRX522661	Sin3a	C2C12	2230	1845/11268	15/11268	123	$<1.0 \times 10^{-324}$	$<1.0 \times 10^{-324}$
6	SRX956815	Six4	C2C12	4850	3510/11268	29/11268	121.034	$<1.0 \times 10^{-324}$	$<1.0 \times 10^{-324}$
7	SRX344972	Sin3a	C2C12	1797	1405/11268	12/11268	117.083	$<1.0 \times 10^{-324}$	$<1.0 \times 10^{-324}$
8	SRX150192	Hdac1	Myoblasts	2823	1217/11268	11/11268	110.636	$<1.0 \times 10^{-324}$	$<1.0 \times 10^{-324}$
9	SRX142525	Max	C2C12	6364	2661/11268	30/11268	88.7	$<1.0 \times 10^{-324}$	$<1.0 \times 10^{-324}$
10	SRX142526	Rest	C2C12	5494	1466/11268	17/11268	86.2353	$<1.0 \times 10^{-324}$	$<1.0 \times 10^{-324}$
(B) TFs similarly distributed with LSD1 (>TSS ± 1 kb)									
1	SRX770038	Myod1	C2C12	4298	3786/40746	60/40746	63.1	$<1.0 \times 10^{-324}$	$<1.0 \times 10^{-324}$
2	SRX142533	Fosl1	C2C12	3696	2664/40746	45/40746	59.2	$<1.0 \times 10^{-324}$	$<1.0 \times 10^{-324}$
3	SRX328690	Myod1	C2C12	10980	8705/40746	153/40746	56.8954	$<1.0 \times 10^{-324}$	$<1.0 \times 10^{-324}$
4	SRX142529	Tcf12	C2C12	7817	6126/40746	112/40746	54.6964	$<1.0 \times 10^{-324}$	$<1.0 \times 10^{-324}$
5	SRX142537	Myod1	C2C12	12521	8722/40746	166/40746	52.5422	$<1.0 \times 10^{-324}$	$<1.0 \times 10^{-324}$
6	SRX142515	Myog	C2C12	5718	4341/40746	84/40746	51.6786	$<1.0 \times 10^{-324}$	$<1.0 \times 10^{-324}$
7	SRX142516	Myod1	C2C12	3446	2568/40746	50/40746	51.36	$<1.0 \times 10^{-324}$	$<1.0 \times 10^{-324}$
8	SRX1817465	Tead4	C2C12	1697	1478/40746	29/40746	50.9655	$<1.0 \times 10^{-324}$	$<1.0 \times 10^{-324}$
9	SRX039346	Epitope tags	C2C12	3133	1462/40746	29/40746	50.4138	$<1.0 \times 10^{-324}$	$<1.0 \times 10^{-324}$
10	SRX213538	Mef2d	C2C12	3551	1840/40746	37/40746	49.7297	$<1.0 \times 10^{-324}$	$<1.0 \times 10^{-324}$

bound promoters (<TSS ± 1 kb) were highly enriched by repressive factors such as Sin3A and Rest in C2C12 cells (Table 1). On the other hand, in genomic regions outside of promoters (>TSS ± 1 kb), myogenic TFs, MyoD (MYOD1) and myogenin (MYOG), were significantly co-localized with LSD1 (Table 1).

We observed that LSD1 was enriched at the promoter regions of oxidative metabolism genes at both days 2 and 5 (Figure 2D and F, Supplementary Figure S5A and B). In addition, LSD1 peaks were also detected in glycolytic genes such as *Gapdh* (Supplementary Figure S5C). LSD1 was bound at about 3 kb upstream of the transcription start site of *Myh7* (Figure 2E and G). LSD1 enrichment was also observed downstream of another slow fiber gene, *Tnnc1* (Supplementary Figure S5D), but not near the fast fiber gene *Myh4* (Supplementary Figure S5E). Interestingly, enrichment of LSD1 at the *Myh7* and *Tnnc1* gene loci was detected at day 2 but not on day 5. In agreement with the ChIP-Atlas results, in the *Myh7* and *Tnnc1* loci, the LSD1 peaks were located at the MyoD- and myogenin-bound sites, which harbored the enhancer box (E-box) sequence, a consensus binding sequence for myogenic TFs (Figure 2E and Supplementary Figure S5D) (27). These results indicate that, in differentiating myoblasts, LSD1 preferentially binds to transcriptionally competent chromatin regions in oxidative fiber-associated genes.

LSD1 inhibition increases H3K4 methylation at target regions of oxidative metabolism genes

To gain mechanistic insights into the role of LSD1 in gene regulation, we analyzed the effects of LSD1 inhibition on expression of LSD1-bound genes. The overall expression profile of LSD1-bound genes was not greatly altered by LSD1 inhibition in C2C12 cells on day 2 (Figure 3A). However, a large percentage of LSD1 inhibition-induced genes (73.1%) was bound to LSD1 (Figure 3B), suggesting that LSD1 was involved in activation of these genes. To evaluate effects of LSD1 inhibition on H3K4 methylation status, we performed ChIP-seq using antibodies against H3K4me1, H3K4me2 and H3K4me3. Most of the genomic regions with high LSD1 enrichment had decreased H3K4me1 levels in the presence of LSD1 inhibition, while H3K4me3 levels were increased (Supplementary Figure S6), suggesting a link between LSD1 activity and H3K4 methylation equilibrium. In the *Pdk4* gene locus, H3K4me2 and H3K4me3 were condensed near the promoter region, while H3K4me1 showed a dispersed distribution, both in control and LSD1-inhibited cells (Figure 3C). By quantitative ChIP-PCR, we observed elevated H3K4me2 levels at the promoters of *Pdk4* and *Atgl* and a relatively high H3K4me3 level at the *Pgc1a* promoter in LSD1-inhibited cells (Figure 3D). In the *Myh7* gene locus, there was widespread distribution of H3K4me1, while H3K4me2 and H3K4me3 were nearly absent (Figure 3E). A region harboring an E-box in *Myh7* did not have detectable redistribution of H3K4 methylation (Figure 3F).

To further confirm regulation of oxidative metabolism genes by LSD1 in myogenic cells, we generated stable LSD1 knockdown (KD) myoblasts by introducing a shRNA expression vector into C2C12 cells (Supplementary Figure S7A). Consistent with previous reports (28–30), LSD1-KD cells failed to differentiate into myotubes upon induction (Supplementary Figure S7B). We performed a microarray analysis of control and LSD1-KD C2C12 cells at differentiation day 2, identifying 2104 genes upregulated by LSD1-KD (Supplementary Figure S7C). Of these, 435 were also upregulated by LSD1 inhibitors and genes in this group were enriched for oxidative genes (Supplementary Figure S7C and D, Supplementary Table S3). By ChIP-qPCR analyses, we found increased H3K4 methylation at a number of oxidative gene promoters and the *Myh7*-E-box region (Supplementary Figure S7E and F). Taken together, these results suggest that loss of LSD1 caused remodeling of local H3K4

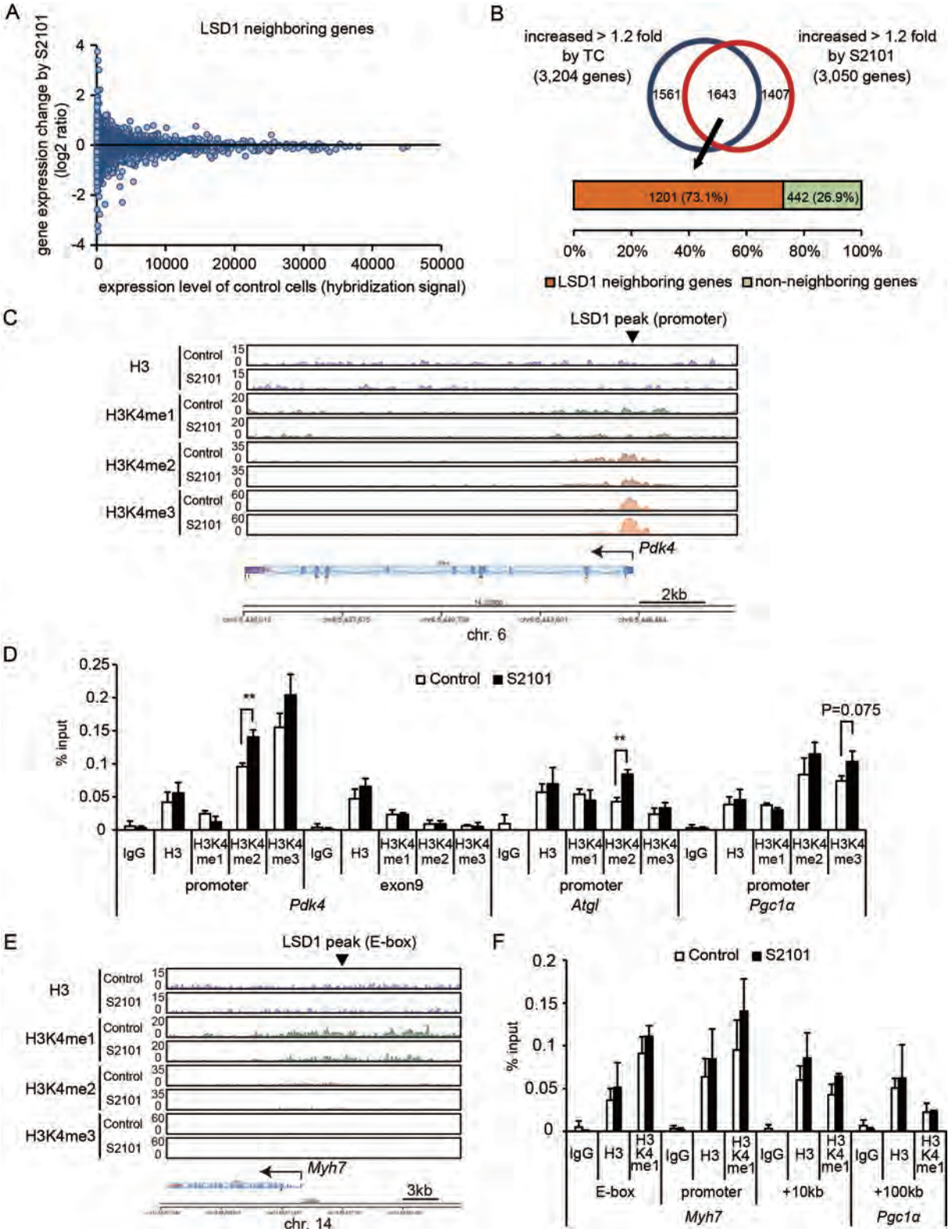

Figure 3. LSD1 fine-tunes expression of actively transcribed genes related to oxidative metabolism. (**A**) Scatterplot showing correlation between gene expression levels and changes in expression under LSD1 inhibition. LSD1-neighboring genes in C2C12 cells on day 2 (16,858 genes) are shown. (**B**) Percentage of LSD1 inhibition-induced genes associated with neighboring LSD1-bound regions. (**C**) H3K4 methylation at the *Pdk4* gene locus. Control or S2101 (10^{-5} M) treated C2C12 cells were analyzed at day 2 after myogenic induction. ChIP-seq data are presented in the same manner as in Figure 2D. (**D**) ChIP-qPCR analyses of H3K4 methylation at metabolic gene promoters. ChIP analyses were performed using differentiating (day 2) C2C12 cells ($n = 3$). (**E**) Histone modifications at the *Myh7* gene locus. (**F**) ChIP-qPCR analyses of H3K4me1 enrichment at the *Myh7* gene locus ($n = 3$). $^{**}P < 0.01$.

dynamics to increase expression of oxidative metabolism genes during myogenesis.

Glucocorticoid induces JADE2-mediated LSD1 degradation

To investigate effects of the endocrine environment on LSD1 activity, we treated differentiated C2C12 myotubes with hormones associated with either anabolic or catabolic signaling. Interestingly, the glucocorticoid analog dexamethasone (Dex) caused a marked decrease in levels of LSD1 protein (Supplementary Figure S8A and B). These results were confirmed by showing a significant decrease in LSD1 levels after Dex treatment in both C2C12 and mouse primary myotubes (Figure 4A and B). Despite the decreased levels of LSD1 protein in the presence of Dex, LSD1 mRNA expression was unaffected, suggesting post-transcriptional regulation (Supplementary Figure S8C and D). It was reported that LSD1 was actively degraded by the ubiquitin-proteasome system (UPS), depending on the cellular context (31,32). To assess the contribution of UPS in Dex-induced LSD1 regulation, cells were treated with MG132, a proteasome inhibitor (Supplementary Figure S9A). To eliminate *de novo* synthesis of LSD1, cycloheximide (CHX) was also added. Combined treatment with MG132 and CHX prevented the suppressive effect of Dex on LSD1 protein levels, indicating that the glucocorticoid triggered proteasomal LSD1 degradation. Several factors were implicated in regulation of LSD1 protein levels. The plant homeodomain finger-containing protein, JADE-2 (also known as PHF15), was reported to act as an E3 ubiquitin ligase for LSD1 in neural cells (31), while USP28 acted as a deubiquitinase for LSD1 in cancer cells (32). Intriguingly, JADE-2 expression was markedly increased in C2C12 and primary myoblasts treated with Dex (Figure 4C–E). A glucocorticoid response element is located at approximately 17 kb upstream of the transcription start site of the *Jade2* gene (33) (Supplementary Figure S9B). By ChIP analysis, we determined that the glucocorticoid receptor (GR) was prominently targeted to this region in response to Dex (Supplementary Figure S9B). To confirm involvement of JADE-2 in Dex-induced LSD1 degradation, we used mouse hepatoma Hepa1-6 cells showing nuclear translocation of abundantly expressed GR (Supplementary Figure S9C). We found that JADE-2 levels were similarly increased by Dex treatment in these cells, and that the Dex-induced decrease in LSD1 levels was attenuated by *Jade2* KD (Supplementary Figure S9D). These data show that glucocorticoid signaling induces JADE-2 expression, resulting in degradation of LSD1 protein.

LSD1 downregulation is mediated by GR in mouse skeletal muscle

Among skeletal muscle tissues in mice, the fast fiber enriched gastrocnemius had higher LSD1 expression than did the slow fiber enriched soleus (Figure 4F, Supplementary Figure S9E). To test glucocorticoid-induced LSD1 suppression *in vivo*, we used muscle-specific glucocorticoid receptor knockout (GRmKO) mice, which exhibited fast fiber enrichment (16). In control mice, continuous administration of Dex for one week induced a moderate decline in LSD1 levels in the skeletal muscle (Figure 4G). In contrast, Dex treatment did not affect LSD1 levels in GRmKO mice (Figure 4G). In agreement with these observations, *Jade2* expression was markedly elevated after continuous Dex treatment, while this effect was attenuated in Dex treated GRmKO mice (Figure 4H). Furthermore, in muscles of adrenalectomized mice, thus devoid of corticosterone production (16), LSD1 levels were significantly elevated (Figure 4I). We next analyzed publicly available transcriptome datasets (34), finding that *Jade2* expression was significantly upregulated in metabolic tissues, such as adipose tissue, liver and skeletal muscle, in fasting mice (Supplementary Figure S9F). These results indicate that LSD1 protein level is negatively regulated by GR-mediated signaling in skeletal muscle.

LSD1 inhibition facilitates glucocorticoid-induced expression of oxidative metabolism genes

Glucocorticoid signaling was shown to enhance OXPHOS and promote the selective wasting of fast muscle fibers (35,36). Having observed that LSD1 repressed expression of oxidative genes (Figure 1), we hypothesized that loss of LSD1 function would enhance the hormonal actions of glucocorticoids. Indeed, Dex treatment during differentiation increased expression of oxidative metabolism genes, an effect further augmented by S2101 (Figure 5A). In addition, LSD1 inhibition and Dex synergistically enhanced expression of the slow fiber gene *Myh7* (Figure 5B and Supplementary Figure S10A). By immunofluorescence, we confirmed that staining with anti-slow-myosin heavy chain (slow-MHC) antibody was enhanced in myotubes treated with Dex and S2101 (Supplementary Figure S10B and C). These data suggest that LSD1 counteracts glucocorticoid-induced expression of oxidative fiber genes. To gain further insights into functional interactions between LSD1 and glucocorticoid signaling, we treated myoblasts with Dex and S2101 during either the early or late phase of differentiation. LSD1 inhibition during the early phase, but not the late phase, markedly augmented Dex-induced expression of both oxidative and *Myh7* genes (Figure 5C and D). These results emphasized that LSD1 contributes to differentiation-coupled metabolic programming in myoblasts.

To explore how LSD1 counteracted glucocorticoid-induced gene expression, we evaluated changes in H3K4 methylation in cells treated with Dex and S2101. H3K4me1 levels were analyzed at the E-box region of the *Myh7* locus, because ChIP-seq data indicated an enrichment of the enhancer signature, including H3K4me1 and acetylated H3K27, at this region (Figure 3E and data not shown) (37). Treatment with S2101, together with Dex, significantly increased H3K4me1 levels at the E-box and at additional regions in the *Myh7* locus (Figure 5E). We also found increased levels of H3K4me2 at the promoter regions of oxidative metabolism genes in cells treated with Dex and S2101, especially at the promoter of *Pgc1α* (Figure 5F). Collectively, our results suggest that LSD1 maintains transcriptionally competent chromatin by H3K4 demethylation, priming these sites for glucocorticoid-induced gene activation.

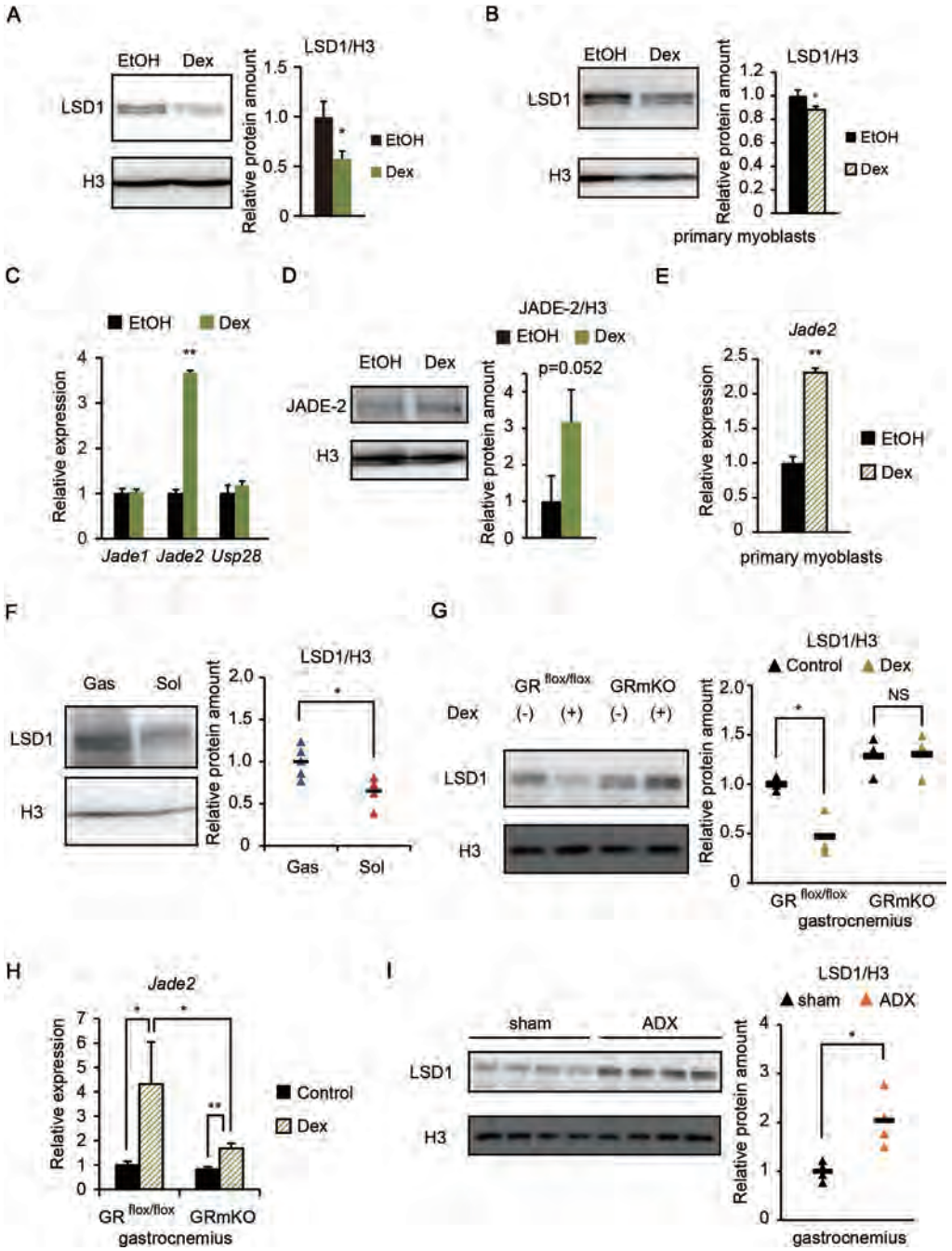

Figure 4. Downregulation of LSD1 by a glucocorticoid in cultured myotubes and in mouse skeletal muscle *in vivo*. (**A** and **B**) Expression of LSD1 protein in C2C12 myotubes (**A**) and primary myoblasts (**B**) under Dex (10^{-6} M) treatment ($n = 3$). Following myogenic induction for 5 days in C2C12 and 4 days in primary cells, cells were treated with Dex or vehicle (EtOH) for 24 h. Band densities were quantified by densitometry and values, normalized to those for histone H3, are shown. (**C**) Expression of genes related to LSD1 ubiquitination ($n = 3$). Cells were subjected to myogenic induction for 4 days and then treated with Dex for 24 h. Values are shown as fold differences against those for EtOH-treated controls. (**D**) Effects of Dex on JADE-2 protein levels in C2C12 myotubes ($n = 3$). Values are shown as fold differences against those for EtOH-treated controls. (**E**) Expression of the *Jade2* gene in myotubes derived from primary myoblasts treated with Dex for 24 h ($n = 3$). (**F**) Expression of LSD1 protein in gastrocnemius (Gas) and soleus (Sol) muscle in 8-week-old male C57BL/6J mice ($n = 5$). Band densities were quantified by densitometry, normalized to those for histone H3 and plotted as triangles. Values are shown as fold differences against the average for Gas. Black bars show the means. (**G**) Effects of Dex administration on LSD1 protein levels in mouse skeletal muscle ($n = 6$). Protein was extracted from Gas muscle from $GR^{flox/flox}$ and GRmKO mice treated with PBS (controls) or Dex for 7 days before sacrifice. Band densities were quantified by densitometry, normalized to those for histone H3 and plotted as triangles. Values are shown as fold differences against the average of vehicle (PBS)-treated $GR^{flox/flox}$ samples. (**H**) Effects of Dex administration on *Jade2* expression in mouse skeletal muscle ($n = 5$). RNA was extracted from Gas muscle from $GR^{flox/flox}$ and GRmKO mice treated with PBS (controls) or Dex for 7 days before sacrifice. Values are shown as fold differences compared with those for PBS-treated $GR^{flox/flox}$ samples. (**I**) Effects of adrenalectomy on LSD1 protein expression in mouse skeletal muscle ($n = 4$). Protein was extracted from Gas muscle from C57BL/6J mice at 7 days after adrenalectomy (ADX) or sham surgery. Band densities were quantified by densitometry and normalized to those for histone H3. Values are shown as fold differences against the averages of sham control samples. $^*P < 0.05$, $^{**}P < 0.01$. NS: no significant difference.

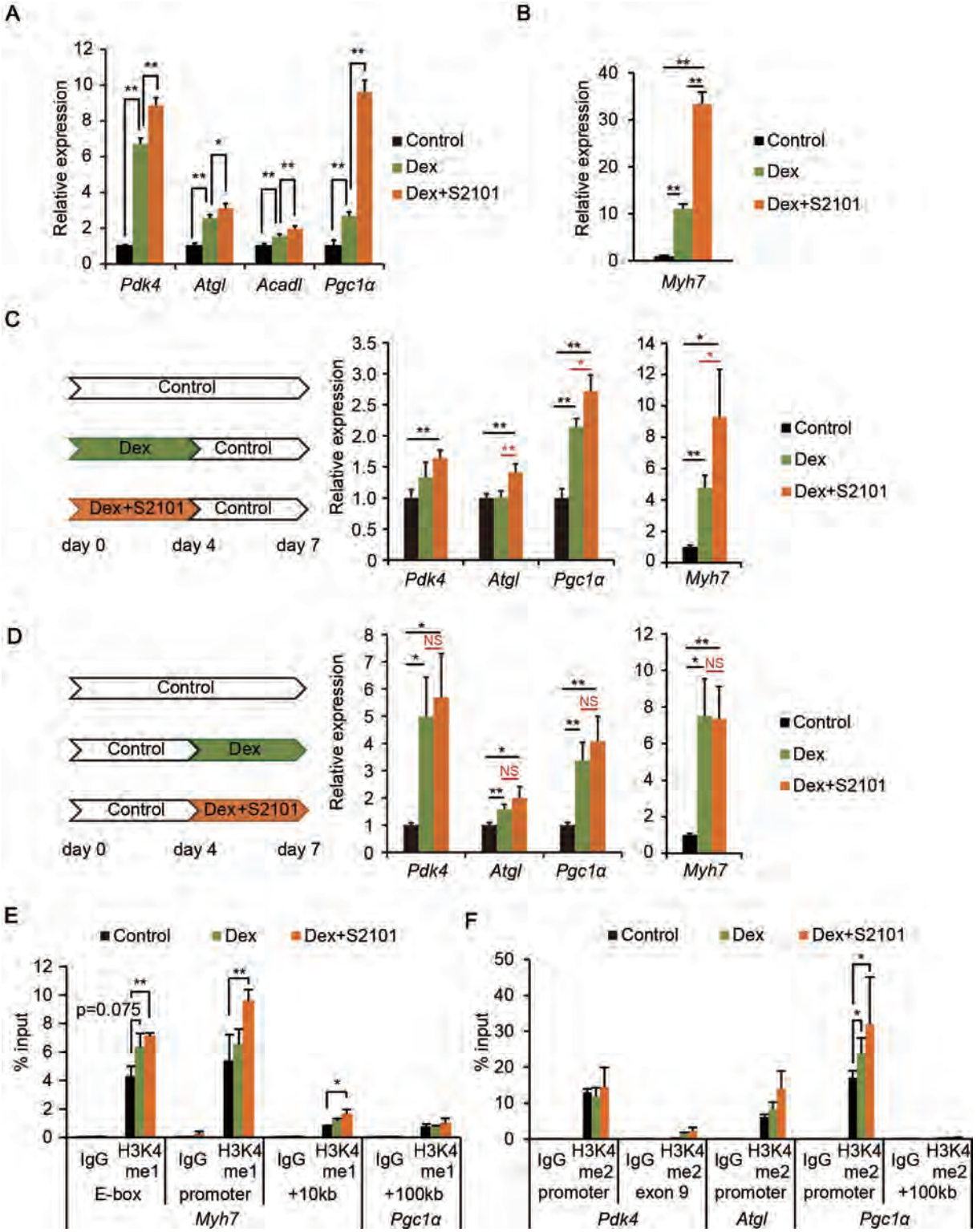

Figure 5. LSD1 inhibition facilitates Dex-induced expression of oxidative genes. (**A**) Effects of Dex and S2101 on expression of oxidative metabolism genes ($n = 3$). C2C12 cells were cultured in differentiation medium for 7 days in the presence of Dex (10^{-6} M) alone or with S2101 (10^{-5} M). Values shown are fold differences against vehicle-treated controls. (**B**) Expression of the *Myh7* gene in Dex- and S2101-treated cells. Values shown are fold differences against vehicle-treated controls. (**C** and **D**) Expression of oxidative metabolism and *Myh7* genes in C2C12 myotubes treated with Dex and S2101 during the early phase (C) or late phase (D) of differentiation ($n = 4$). RNA was extracted from C2C12 cells on day 7 after differentiation with the indicated treatments. (**E**) Enrichment of H3K4me1 at the *Myh7* gene locus. ChIP analyses were performed using differentiating C2C12 cells (48 h) treated with Dex and S2101 ($n = 3$). Values are each shown as % input. (**F**) Enrichment of H3K4me2 at the promoter regions of oxidative metabolism genes. $^{*}P < 0.05$, $^{**}P < 0.01$. NS: no significant difference.

DISCUSSION

Environmental conditions, such as nutritional state, exert profound influences on epigenome, but little is known about the underlying mechanisms. Our study demonstrated that LSD1 transcriptionally repressed oxidative metabolism and slow fiber myosin genes via the H3K4 demethylation, with a concomitant decrease of oxygen consumption. A catabolic glucocorticoid signal decreased LSD1 protein levels by the glucocorticoid receptor-mediated expression of the E3 ubiquitin ligase, JADE-2. In agreement with these observations, the combination of glucocorticoid stimulation and LSD1 inhibition synergistically enhanced oxidative fiber gene expression with increased levels of H3K4 methylation at LSD1-bound promoters and enhancers. These results indicated that LSD1 serves as an epigenetic hub to translate environmental information into epigenetic remodeling (Supplementary Figure S11).

Previous reports showed that LSD1 was required for differentiation of cultured myoblasts (28,29). Those findings were based on LSD1 loss-of-function experiments using stable shRNA expression or CRSPR-Cas9-based genome editing, which required extended culture of undifferentiated myoblasts after LSD1 inactivation. This extended culture might have significantly affected the myogenic potential of the cells. More recently, Scionti *et al.* reported that LSD1 was required for MyoD expression at the initial step of myogenesis in myogenic stem cells (30). Notably, they demonstrated that H3K9 methylation level at an enhancer of *Myod* gene was increased in LSD1-KD cells before differentiation induction, suggesting that those cells had lost myogenic identity. Consistent with these previous reports, we observed a loss of differentiation potential after establishment of LSD1-KD in C2C12 cells, accompanied by decreased MyoD expression (Supplementary Figure S7 and data not shown). In our study, we demonstrated that LSD1 restricted the metabolic properties of differentiating myoblasts by suppressing expression of oxidative genes without affecting the differentiation itself. Of note, we added LSD1 inhibiting drugs only during the differentiation period, when MyoD expression had already been established. Scionti et al. tested the effects of LSD1 inhibitors other than the ones we used, and demonstrated that inhibitor treatment upon differentiation did not affect *Myod* expression (30). Thus, both our study and previous reports demonstrated that LSD1 function during myogenesis depends on the differentiation state. In particular, our data show that LSD1 has context-dependent activities as an environment-responsive epigenetic factor.

LSD1 contributes to repressive chromatin structure through H3K4 demethylation, but in some cases, activates transcription through H3K9 demethylation (8,38). Our ChIP-seq data revealed that LSD1 was highly coincident with active chromatin marks such as methylated H3K4, H3K27ac and pol II, suggesting that LSD1 preferentially binds to transcriptionally competent chromatin. At genomic regions with high LSD1 occupancy, loss of LSD1 activity was associated with reduced H3K4me1 and increased H3K4me3 levels. At oxidative metabolism gene loci, loss of LSD1 led to upregulated expression with moderate increase in H3K4 methylation. By contrast, LSD1 did not show a prominent engagement with H3K9me3 peaks. We previously reported using adipogenic cells that LSD1 inhibition did not affect H3K9 methylation at the promoters of oxidative metabolism genes (9). Collectively, the line of evidences suggests that, for the regulation of metabolic plasticity, LSD1 contribute to the balancing of H3K4 methylation state at transcriptionally competent genes, rather than affecting tightly repressive H3K9 methylation marks. LSD2, the other flavin-dependent lysine demethylase, is also expressed in myogenic cells (data not shown). We previously reported that LSD2 repressed lipid transport genes including *CD36* to limit lipid influx and metabolism in human hepatic cells (39). Previous report demonstrated that CD36 was preferentially expressed in slow-twitch rather than fast-twitch fiber of human skeletal muscle (40). Thus, LSD2 together with LSD1 might contribute to the suppression of slow type metabolism in the muscle.

A glucocorticoid was shown to enhance oxidative metabolism and contractility in fetal cardiomyocytes by inducing expression of the *PGC-1*α gene (41). In addition, glucocorticoid signaling promotes fast fiber-selective muscle wasting, suggesting that this class of hormones favored oxidative muscle activity (36,42). Here, we demonstrated that Dex treatment led to increased expression of oxidative and slow-type myosin genes, effects further augmented by LSD1 inhibition. Our results suggest that the catabolic action of the glucocorticoid in muscle was counteracted by LSD1-mediated chromatin modification. Also of interest, a glucocorticoid surge in late gestation was reported to contribute to maturation of cardiac muscle, which shows a high bias toward oxidative energy metabolism (43). Thus, it is possible that crosstalk between glucocorticoids and LSD1 may be involved in early programming of oxidative capacity in muscle lineages.

Epidemiologic and animal studies indicated that malnutrition or over-nutrition in early life is linked to an increased risk of metabolic disorders such as obesity, diabetes and cardiovascular diseases in adulthood (44,45). Although relationships between diet and the epigenome have been very actively studied, it is not yet clear how nutritional conditions can affect health and disease through specific epigenetic mechanisms (3). Previously, we demonstrated that, under anabolic conditions, LSD1 repressed expression of oxidative metabolism and lipid metabolism associated genes in cultured adipose cells and tissues (9,10). Our current study further showed that glucocorticoids, involved in fetal and postnatal growth in mammals, targeted LSD1-mediated metabolic gene regulation. Interestingly, patients with type 2 diabetes or obesity were reported to have more glycolytic and fewer oxidative fibers, compared with healthy individuals (46,47). In addition, the *PGC-1*α gene was epigenetically silenced in the skeletal muscle of individuals with diabetes (48). Based on these findings, it is tempting to speculate that the nutritional environment could influence LSD1-mediated epigenome formation, which may then affect long-term metabolic outcomes.

In conclusion, our study demonstrated that multiple metabolic signaling processes affect LSD1 activity, which could then influence the trajectory of metabolic reprogramming in differentiating myoblasts. Our findings extend the

current understanding of how environmental factors can control the epigenome during transitions of cellular states.

DATA AVAILABILITY

The accession number for the microarray data presented in this paper are GEO: GSE86524 (LSD1 inhibitors) and GSE109839 (LSD1-KD), and that for the ChIP-seq data are GSE109845 (methylated H3K4) and GSE109846 (LSD1).

SUPPLEMENTARY DATA

Supplementary Data are available at NAR Online.

ACKNOWLEDGEMENTS

We thank our laboratory members for helpful discussions and technical support. We thank Susan R. Doctrow, PhD, from Edanz Group (www.edanzediting.com/ac) for editing a draft of this manuscript.
Author Contributions: Conceptualization, K.A., S.H. and M.N.; Methodology, K.A. and S.H.; Software, S.O.; Investigation, K.A., S.H., N.S., A.K., K.N., R.T., K.K., H.A., Y.H and S.U.; Writing, K.A., S.H., N.S. and M.N.; Visualization, K.A., S.H. and M.N.; Supervision, H.T., K.N., F.E. and M.N.; Funding acquisition, S.H. and M.N.

FUNDING

JSPS KAKENHI [JP15H04707 to M.N., JP15K15068 to M.N., JP16K07215 to S.H., 25430178 to S.H.]; Takeda Science Foundation (to M.N. and S.H.); Kanae Foundation for the Promotion of Medical Science (to S.H.); Ono Medical Research Foundation (to S.H.); Mochida Memorial Foundation for Medical and Pharmaceutical Research (to S.H.). Funding for open access charge: Takeda Science Foundation.
Conflict of interest statement. None declared.

REFERENCES

1. Feil,R. and Fraga,M.F. (2011) Epigenetics and the environment: emerging patterns and implications. *Nat. Rev. Genet.*, **13**, 97–109.
2. Siebel,A.L., Fernandez,A.Z. and El-Osta,A. (2010) Glycemic memory associated epigenetic changes. *Biochem. Pharmacol.*, **80**, 1853–1859.
3. Jimenez-Chillaron,J.C., Diaz,R., Martinez,D., Pentinat,T., Ramon-Krauel,M., Ribo,S. and Plosch,T. (2012) The role of nutrition on epigenetic modifications and their implications on health. *Biochimie*, **94**, 2242–2263.
4. Burg,J.M., Link,J.E., Morgan,B.S., Heller,F.J., Hargrove,A.E. and McCafferty,D.G. (2015) KDM1 class flavin-dependent protein lysine demethylases. *Biopolymers*, **104**, 213–246.
5. Shi,Y., Lan,F., Matson,C., Mulligan,P., Whetstine,J.R., Cole,P.A., Casero,R.A. and Shi,Y. (2004) Histone demethylation mediated by the nuclear amine oxidase homolog LSD1. *Cell*, **119**, 941–953.
6. Amente,S., Lania,L. and Majello,B. (2013) The histone LSD1 demethylase in stemness and cancer transcription programs. *Biochim. Biophys. Acta.*, **1829**, 981–986.
7. Hino,S., Nagaoka,K. and Nakao,M. (2013) Metabolism-epigenome crosstalk in physiology and diseases. *J. Hum. Genet.*, **58**, 410–415.
8. Hino,S., Kohrogi,K. and Nakao,M. (2016) Histone demethylase LSD1 controls the phenotypic plasticity of cancer cells. *Cancer Sci.*, **107**, 1187–1192.
9. Hino,S., Sakamoto,A., Nagaoka,K., Anan,K., Wang,Y., Mimasu,S., Umehara,T., Yokoyama,S., Kosai,K. and Nakao,M. (2012) FAD-dependent lysine-specific demethylase-1 regulates cellular energy expenditure. *Nat. Commun.*, **3**, 758.
10. Sakamoto,A., Hino,S., Nagaoka,K., Anan,K., Takase,R., Matsumori,H., Ojima,H., Kanai,Y., Arita,K. and Nakao,M. (2015) Lysine Demethylase LSD1 coordinates glycolytic and mitochondrial metabolism in hepatocellular carcinoma cells. *Cancer Res.*, **75**, 1445–1456.
11. Duteil,D., Metzger,E., Willmann,D., Karagianni,P., Friedrichs,N., Greschik,H., Gunther,T., Buettner,R., Talianidis,I., Metzger,D. *et al.* (2014) LSD1 promotes oxidative metabolism of white adipose tissue. *Nat. Commun.*, **5**, 4093.
12. Schiaffino,S. and Reggiani,C. (2011) Fiber types in mammalian skeletal muscles. *Physiol. Rev.*, **91**, 1447–1531.
13. Hoppeler,H. (2016) Molecular networks in skeletal muscle plasticity. *J. Exp. Biol.*, **219**, 205–213.
14. Moresi,V., Marroncelli,N. and Adamo,S. (2015) New insights into the epigenetic control of satellite cells. *World J. Stem. Cells*, **7**, 945–955.
15. Carrio,E. and Suelves,M. (2015) DNA methylation dynamics in muscle development and disease. *Front Aging Neurosci.*, **7**, 19.
16. Shimizu,N., Maruyama,T., Yoshikawa,N., Matsumiya,R., Ma,Y., Ito,N., Tasaka,Y., Kuribara-Souta,A., Miyata,K., Oike,Y. *et al.* (2015) A muscle-liver-fat signalling axis is essential for central control of adaptive adipose remodelling. *Nat. Commun.*, **6**, 6693.
17. Rando,T.A. and Blau,H.M. (1994) Primary mouse myoblast purification, characterization, and transplantation for cell-mediated gene therapy. *J. Cell Biol.*, **125**, 1275–1287.
18. Li,H. and Durbin,R. (2009) Fast and accurate short read alignment with Burrows-Wheeler transform. *Bioinformatics*, **25**, 1754–1760.
19. Zhang,Y., Liu,T., Meyer,C.A., Eeckhoute,J., Johnson,D.S., Bernstein,B.E., Nusbaum,C., Myers,R.M., Brown,M., Li,W. *et al.* (2008) Model-based analysis of ChIP-Seq (MACS). *Genome Biol.*, **9**, R137.
20. Lee,M.G., Wynder,C., Schmidt,D.M., McCafferty,D.G. and Shiekhattar,R. (2006) Histone H3 lysine 4 demethylation is a target of nonselective antidepressive medications. *Chem. Biol.*, **13**, 563–567.
21. Mimasu,S., Umezawa,N., Sato,S., Higuchi,T., Umehara,T. and Yokoyama,S. (2010) Structurally designed trans-2-phenylcyclopropylamine derivatives potently inhibit histone demethylase LSD1/KDM1. *Biochemistry*, **49**, 6494–6503.
22. Niwa,H. and Umehara,T. (2017) Structural insight into inhibitors of flavin adenine dinucleotide-dependent lysine demethylases. *Epigenetics*, **12**, 340–352.
23. Bentzinger,C.F., Wang,Y.X. and Rudnicki,M.A. (2012) Building muscle: molecular regulation of myogenesis. *Cold Spring Harb. Perspect. Biol.*, **4**, a008342.
24. Subramanian,A., Tamayo,P., Mootha,V.K., Mukherjee,S., Ebert,B.L., Gillette,M.A., Paulovich,A., Pomeroy,S.L., Golub,T.R., Lander,E.S. *et al.* (2005) Gene set enrichment analysis: a knowledge-based approach for interpreting genome-wide expression profiles. *Proc. Natl. Acad. Sci. U.S.A.*, **102**, 15545–15550.
25. Watt,M.J. and Hoy,A.J. (2012) Lipid metabolism in skeletal muscle: generation of adaptive and maladaptive intracellular signals for cellular function. *Am. J. Physiol. Endocrinol. Metab.*, **302**, E1315–E1328.
26. Yuan,Y., Shi,X.E., Liu,Y.G. and Yang,G.S. (2011) FoxO1 regulates muscle fiber-type specification and inhibits calcineurin signaling during C2C12 myoblast differentiation. *Mol. Cell. Biochem.*, **348**, 77–87.
27. Moncaut,N., Rigby,P.W. and Carvajal,J.J. (2013) Dial M(RF) for myogenesis. *FEBS J.*, **280**, 3980–3990.
28. Choi,J., Jang,H., Kim,H., Kim,S.T., Cho,E.J. and Youn,H.D. (2010) Histone demethylase LSD1 is required to induce skeletal muscle differentiation by regulating myogenic factors. *Biochem. Biophys. Res. Commun.*, **401**, 327–332.
29. Munehira,Y., Yang,Z. and Gozani,O. (2017) Systematic analysis of known and candidate lysine demethylases in the regulation of myoblast differentiation. *J. Mol. Biol.*, **429**, 2055–2065.
30. Scionti,I., Hayashi,S., Mouradian,S., Girard,E., Esteves de Lima,J., Morel,V., Simonet,T., Wurmser,M., Maire,P., Ancelin,K. *et al.* (2017) LSD1 controls timely MyoD expression via MyoD core enhancer transcription. *Cell Rep.*, **18**, 1996–2006.

31. Han,X., Gui,B., Xiong,C., Zhao,L., Liang,J., Sun,L., Yang,X., Yu,W., Si,W., Yan,R. *et al.* (2014) Destabilizing LSD1 by Jade-2 promotes neurogenesis: an antibraking system in neural development. *Mol. Cell*, **55**, 482–494.
32. Wu,Y., Wang,Y., Yang,X.H., Kang,T., Zhao,Y., Wang,C., Evers,B.M. and Zhou,B.P. (2013) The deubiquitinase USP28 stabilizes LSD1 and confers stem-cell-like traits to breast cancer cells. *Cell Rep.*, **5**, 224–236.
33. Kuo,T., Lew,M.J., Mayba,O., Harris,C.A., Speed,T.P. and Wang,J.C. (2012) Genome-wide analysis of glucocorticoid receptor-binding sites in myotubes identifies gene networks modulating insulin signaling. *Proc. Natl. Acad. Sci. U.S.A.*, **109**, 11160–11165.
34. Schupp,M., Chen,F., Briggs,E.R., Rao,S., Pelzmann,H.J., Pessentheiner,A.R., Bogner-Strauss,J.G., Lazar,M.A., Baldwin,D. and Prokesch,A. (2013) Metabolite and transcriptome analysis during fasting suggest a role for the p53-Ddit4 axis in major metabolic tissues. *BMC Genomics*, **14**, 758.
35. Lee,S.R., Kim,H.K., Song,I.S., Youm,J., Dizon,L.A., Jeong,S.H., Ko,T.H., Heo,H.J., Ko,K.S., Rhee,B.D. *et al.* (2013) Glucocorticoids and their receptors: insights into specific roles in mitochondria. *Prog. Biophys. Mol. Biol.*, **112**, 44–54.
36. Shimizu,N., Yoshikawa,N., Ito,N., Maruyama,T., Suzuki,Y., Takeda,S., Nakae,J., Tagata,Y., Nishitani,S., Takehana,K. *et al.* (2011) Crosstalk between glucocorticoid receptor and nutritional sensor mTOR in skeletal muscle. *Cell Metab.*, **13**, 170–182.
37. Zhou,V.W., Goren,A. and Bernstein,B.E. (2011) Charting histone modifications and the functional organization of mammalian genomes. *Nat. Rev. Genet.*, **12**, 7–18.
38. Metzger,E., Wissmann,M., Yin,N., Muller,J.M., Schneider,R., Peters,A.H., Gunther,T., Buettner,R. and Schule,R. (2005) LSD1 demethylates repressive histone marks to promote androgen-receptor-dependent transcription. *Nature*, **437**, 436–439.
39. Nagaoka,K., Hino,S., Sakamoto,A., Anan,K., Takase,R., Umehara,T., Yokoyama,S., Sasaki,Y. and Nakao,M. (2015) Lysine-specific demethylase 2 suppresses lipid influx and metabolism in hepatic cells. *Mol. Cell. Biol.*, **35**, 1068–1080.
40. Vistisen,B., Roepstorff,K., Fau-Roepstorff,C., Roepstorff,C., Fau-Bonen,A., Bonen,A., Fau-van Deurs,B., van Deurs,B., Fau-Kiens,B. and Kiens,B. (2004) Sarcolemmal FAT/CD36 in human skeletal muscle colocalizes with caveolin-3 and is more abundant in type 1 than in type 2 fibers. *J. Lipid Res.*, **45**, 603–609.
41. Rog-Zielinska,E.A., Craig,M.A., Manning,J.R., Richardson,R.V., Gowans,G.J., Dunbar,D.R., Gharbi,K., Kenyon,C.J., Holmes,M.C., Hardie,D.G. *et al.* (2015) Glucocorticoids promote structural and functional maturation of foetal cardiomyocytes: a role for PGC-1alpha. *Cell Death Differ.*, **22**, 1106–1116.
42. Ciciliot,S., Rossi,A.C., Dyar,K.A., Blaauw,B. and Schiaffino,S. (2013) Muscle type and fiber type specificity in muscle wasting. *Int. J. Biochem. Cell Biol.*, **45**, 2191–2199.
43. Rog-Zielinska,E.A., Richardson,R.V., Denvir,M.A. and Chapman,K.E. (2014) Glucocorticoids and foetal heart maturation; implications for prematurity and foetal programming. *J. Mol. Endocrinol.*, **52**, R125–R135.
44. Hales,C.N. and Barker,D.J. (2001) The thrifty phenotype hypothesis. *Br. Med. Bull.*, **60**, 5–20.
45. Roseboom,T.J., van der Meulen,J.H., Ravelli,A.C., Osmond,C., Barker,D.J. and Bleker,O.P. (2001) Effects of prenatal exposure to the Dutch famine on adult disease in later life: an overview. *Mol. Cell. Endocrinol.*, **185**, 93–98.
46. He,J., Watkins,S. and Kelley,D.E. (2001) Skeletal muscle lipid content and oxidative enzyme activity in relation to muscle fiber type in type 2 diabetes and obesity. *Diabetes*, **50**, 817–823.
47. Tanner,C.J., Barakat,H.A., Dohm,G.L., Pories,W.J., MacDonald,K.G., Cunningham,P.R., Swanson,M.S. and Houmard,J.A. (2002) Muscle fiber type is associated with obesity and weight loss. *Am. J. Physiol. Endocrinol. Metab.*, **282**, E1191–E1196.
48. Barres,R., Osler,M.E., Yan,J., Rune,A., Fritz,T., Caidahl,K., Krook,A. and Zierath,J.R. (2009) Non-CpG methylation of the PGC-1alpha promoter through DNMT3B controls mitochondrial density. *Cell Metab*, **10**, 189–198.

Supplementary Data

Title:

LSD1 mediates metabolic reprogramming by glucocorticoids during myogenic differentiation

Authors:

Kotaro Anan[1,2], Shinjiro Hino[1*], Noriaki Shimizu[4], Akihisa Sakamoto[1], Katsuya Nagaoka[1], Ryuta Takase[1], Kensaku Kohrogi[1,2], Hirotaka Araki[1], Yuko Hino[1], Shingo Usuki[3], Shinya Oki[5], Hirotoshi Tanaka[4], Kimitoshi Nakamura[2], Fumio Endo[2], and Mitsuyoshi Nakao[1*]

Affiliations:

[1]Department of Medical Cell Biology, Institute of Molecular Embryology and Genetics,
[2]Department of Pediatrics, Graduate School of Medical Sciences,
[3]Liaison Laboratory Research Promotion Center, Institute of Molecular Embryology and Genetics, Kumamoto University, Kumamoto 860-0811, Japan
[4]Division of Rheumatology, Center for Antibody and Vaccine Therapy, IMSUT Hospital, The Institute of Medical Science, The University of Tokyo, Tokyo 108-8639, Japan
[5]Department of Developmental Biology, Graduate school of Medical Sciences, Kyushu University, Fukuoka 812-8582, Japan

***Corresponding Authors:**

Shinjiro Hino Ph.D. (s-hino@kumamoto-u.ac.jp)
Mitsuyoshi Nakao M.D., Ph.D. (mitnakao@kumamoto-u.ac.jp)
Department of Medical Cell Biology,
Institute of Molecular Embryology and Genetics, Kumamoto University
2-2-1 Honjo, Chuo-ku, Kumamoto 860-0811, Japan.
Phone: +81-96-373-6800; Fax: +81-96-373-6804

SUPPLEMENTARY FIGURE LEGENDS

Supplementary Figure S1. LSD1 inhibition that does not interfere with myogenic differentiation. (**A**) Experimental procedures used: C2C12 mouse myoblasts were differentiated to myotubes in the absence or presence of LSD1 inhibition and then subjected to the indicated analyses. (**B**) Expression levels of differentiation marker genes in day 7-C2C12 cells treated with LSD1 inhibitors (n = 4). Quantitative RT-PCR data were normalized to values for the *36B4* gene, shown as fold differences against vehicle-treated controls. Concentrations of TC and S2101 were 10^{-4} and 10^{-5} M, respectively. (**C**) Myogenic differentiation of C2C12 cells under LSD1 inhibition. Cells were prepared as described for (**A**). Myotube formation was analyzed by immunofluorescence imaging of myosin heavy chain (MHC). Scale bar, 100 μm. (**D**) Quantitative analyses of myotube formation under S2101 treatment. The number of nuclei, ratio of MHC-expressing nuclei to total nuclei, and area and intensity of the MHC signal are shown for control and S2101-treated cells. Values are means ± s.d. of 3 assay wells. For each well, 30 fields were counted.

Supplementary Figure S2. Effects of LSD1 inhibition on gene expression in differentiating myoblasts. (**A**) GSEA results for genes upregulated by LSD1 inhibition. Fourteen pathways were identified with statistically significant differences (p-value < 0.05 and FDR q-value < 0.25). Pathways related to lipid metabolism are highlighted in red. (**B**) Venn diagram of the genes with expression decreased by 1.5-fold or more by treatment with LSD1 inhibitors, TC or S2101 (left). Cells were collected at 48 h after myogenic induction. Controls were treated with vehicle. GSEA results for genes downregulated by LSD1 inhibition (right). Five pathways were identified with

statistically significant differences (p-value < 0.05 and FDR q-value < 0.25).

Supplementary Figure S3. Effects of LSD1 inhibition on metabolic properties of C2C12 cells. (**A** and **B**) Effects of LSD1 inhibition on the OXPHOS capacity of differentiated C2C12 cells. OCR/ECAR: the ratio of oxygen consumption rate (OCR, **Figure 1E**) to extracellular acidification rate (ECAR) (A) and ECAR (B) are shown (n = 10). During real-time measurements, respiratory chain inhibitors were added to the medium at the indicated time points. Values are means ± s.d. (**C**) Heatmap showing expression change of glycolysis related genes in LSD1-inhibited C2C12 cells. Expression data were extracted from microarray analyses described in **Figure 1A** and **S7**. Values are shown as fold differences against the average of each control. *p < 0.05, **p < 0.01.

Supplementary Figure S4. LSD1 enrichment relative to histone modifications and RNA polymerase II peaks on day 2 (**A**) or 5 (**B**). Data are presented in the same manner as for **Figure 2C**.

Supplementary Figure S5. Distribution of LSD1-bound sites in differentiating (day 2) or differentiated (day 5) myoblasts. Enrichment of LSD1 at the oxidative *Atgl* (**A**) and *Pgc1α* (**B**) genes, the glycolytic *Gapdh* (**C**) gene and the slow fiber-associated *Tnnc1* (**D**) gene loci. (**E**) No enrichment of LSD1 at the fast fiber-associated *Myh4* gene locus. ChIP-seq data were visualized using Strand NGS software (Strand Genomics). Histone modifications at the *Pgc1α* (B) and *Tnnc1* (D) gene loci in control cells (described in **Figure 3C**) and publicly available ChIP-seq data for Rest, Max, Six4, MyoD and

myogenin are also shown (Data IDs are listed in **MATERIALS AND METHODS**).

Supplementary Figure S6. Scatter plots show the correlation between LSD1 enrichment and changes in H3K4 methylation by LSD1 inhibition. LSD1-enriched regions in C2C12 cells (day 2) are shown. The x-axis shows the enrichment levels of LSD1 in these regions and the y-axis shows changes in H3K4me1 (**A**), H3K4me2 (**B**) and H3K4me3 (**C**) enrichment levels induced by LSD1 inhibition. Enrichment values were normalized over input and are shown as log2 ratio. The areas with more than 2.5 log values in the x-axis and with more than 0.5 or less than -0.5 log values in the y-axis are indicated by boxes. The region numbers included in each area are shown.

Supplementary Figure S7. Effects of LSD1 knockdown in C2C12 myoblasts. (**A**) LSD1 expression in shRNA-introduced cells. Protein was collected from C2C12 cells stably expressing shRNA at 48 h after myogenic induction. (**B**) Light microscope images of LSD1-KD C2C12 cells. sh*Lsd1*- or shControl-expressing C2C12 cells were analyzed at 7 d after myogenic induction. Scale bar, 500 μm. (**C**) Venn diagram of the genes induced by 1.2-fold or more by LSD1-KD and LSD1-bound genes with expression upregulated by LSD1 inhibitors (**Figure 3B**). Microarray analysis was performed in sh*Lsd1*-expressing C2C12 cells at 48 h after myogenic induction. (**D**) Expression levels of oxidative metabolism and myogenesis genes in LSD1-KD cells at 48 h after myogenic induction (n = 3). Values are shown as fold differences against control shRNA-expressing samples. (**E** and **F**) H3K4me1 (E) and H3K4me2 (F) enrichment at LSD1-bound regions in LSD1-KD C2C12 cells. ChIP-qPCR analyses were performed in sh*Lsd1*-expressing C2C12 cells at 48 h after myogenic induction.

Values are means ± s.d. *$p < 0.05$, **$p < 0.01$.

Supplementary Figure S8. Glucocorticoid treatment decreases the amount of LSD1 protein. (**A**) Procedures for sample preparation: C2C12 mouse myoblasts were differentiated to myotubes, then treated with hormones before being subjected to RNA and protein analyses. (**B**) Expression of LSD1 protein in C2C12 myotubes under various hormone treatments. Administered hormones were T: testosterone (10^{-8} M), E2: estradiol (10^{-8} M), Ins: insulin (10^{-7} M), EtOH: ethanol vehicle (0.1%), Dex: dexamethasone (10^{-6} M) and T3: triiodothyronine (10^{-8} M). Band densities were quantified by densitometry and normalized to those for histone H3. Values are shown as fold differences against those for the vehicle EtOH-treated control. (**C** and **D**) Expression of *LSD1* mRNA in C2C12 myotubes (C) and primary myoblasts (D) under Dex treatment (n = 3). qRT-PCR values are presented as fold differences, against those for vehicle treated controls. Values are means ± s.d. NS: no significant difference.

Supplementary Figure S9. Glucocorticoid-induced *Jade2* expression results in LSD1 degradation. (**A**) Effect of proteasome inhibition on LSD1 protein under Dex treatment (n = 3). C2C12 cells were differentiated for 48 h and then treated with Dex (10^{-6} M) for 24 h. Cells were also treated with cycloheximide (CHX, 100 μg/mL) and MG132 (10^{-5} M) for 6 h before harvest. (**B**) Glucocorticoid receptor (GR) occupancy the *Jade2* gene locus. ChIP analyses were performed using differentiating C2C12 cells treated with Dex for 48 h (n = 3). Numbers 1–6 indicate the sites used for qPCR experiments. Fold enrichment values were calculated relative to control IgG. (**C**) Nuclear accumulation of GR upon Dex treatment in Hepa1-6 cells. GR expression and accumulation into nuclei

was analyzed by immunofluorescence staining, using cells treated with EtOH (control) or Dex for 24 h. Scale bar, 10 μm. (**D**) Effect of Jade2 knockdown on LSD1 protein under Dex treatment (n = 3). Hepa1-6 cells were transfected with si*Jade2*. At 24 h after transfection, cells were treated with Dex (10^{-6} M) for 48 h, together with CHX (100 μg/mL) for 6 h before harvesting samples. Target sequences of siRNA are shown in **MATERIALS AND METHODS**. (**E**) Expression of *LSD1* mRNA in gastrocnemius (Gas) and soleus (Sol) (n = 5). qRT-PCR values are presented as fold differences relative to those for Gas. (**F**) Expression of *Jade2* gene in fasted mice (n = 5). Microarray data from a public database (NCBI GSE46495) was used to calculate *Jade2* expression in mouse tissues after 24 h fasting. Values are fold differences against those for *ad libitum* fed mice, means ± s.d. **p* < 0.05, ***p* < 0.01. NS: no significant difference.

Supplementary Figure S10. Treatment with Dex activates slow myosin expression. (**A**) Expression levels of myosin genes in C2C12 myotubes treated with Dex and S2101 (n = 3). Values are fold differences against vehicle-treated controls. (**B**) Expression of slow-myosin heavy chain (slow-MHC) in Dex- and S2101-treated cells. C2C12 cells on myogenic day 5 were analyzed by immunofluorescence microscopy. Scale bar, 100 μm. (**C**) Quantitative analyses of the images obtained in (B). The areas of slow-MHC signal, intensities of slow-MHC signal and the ratios of these parameters are shown. Values are means ± s.d. of 3 assay wells. For each well, 30 fields were counted. Values are means ± s.d. **p* < 0.05, ***p* < 0.01, ****p* < 0.001.

Supplementary Figure S11. Schematic model of LSD1-mediated metabolic programming in differentiating myoblasts under the action of a glucocorticoid. Glucocorticoid via the glucocorticoid receptor (GR) induces expression of JADE-2, a ubiquitin E3 ligase for LSD1, resulting in de-repression of the target genes involved in oxidative metabolism.

Supplementary Figure S12. Uncropped western blot membranes presented in this study. Areas surrounded by black boxes are those shown in individual figures.

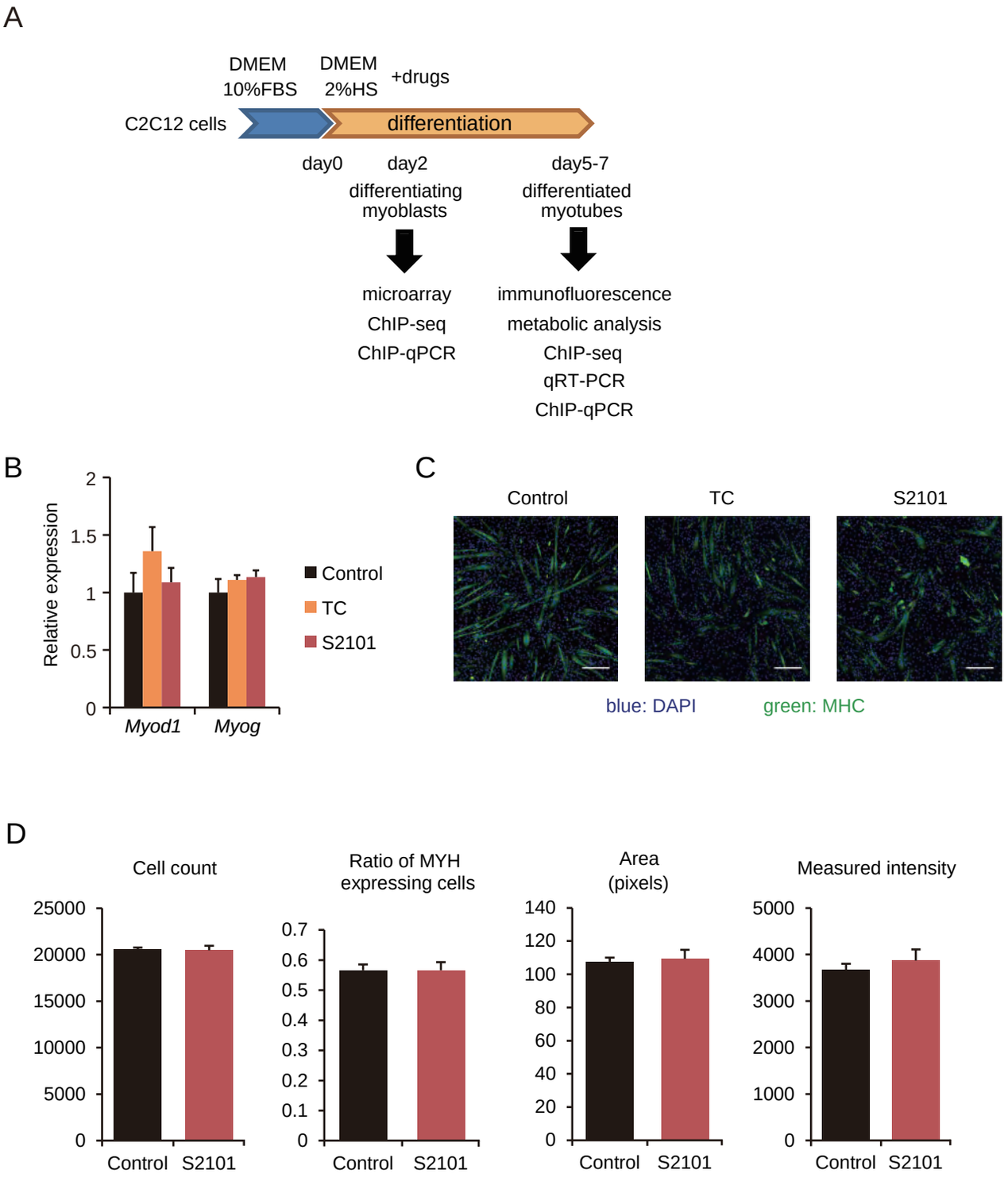

Anan *et al.* Figure S1

A

upregulated by LSD1 inhibition

NAME	NOM p-value	FDR q-value
KEGG_STEROID_BIOSYNTHESIS	<0.001	0.007131594
KEGG_LYSOSOME	<0.001	0.007186448
KEGG_GLUTATHIONE_METABOLISM	<0.001	0.008344005
KEGG_SPHINGOLIPID_METABOLISM	0.002631579	0.01331426
KEGG_DRUG_METABOLISM_CYTOCHROME_P450	0.002604167	0.013592466
KEGG_BIOSYNTHESIS_OF_UNSATURATED_FATTY_ACIDS	0.014117647	0.1463684
KEGG_METABOLISM_OF_XENOBIOTICS_BY_CYTOCHROME_P450	0.02676399	0.15217118
KEGG_EPITHELIAL_CELL_SIGNALING_IN_HELICOBACTER_PYLORI_INFECTION	0.005347594	0.15309496
KEGG_FATTY_ACID_METABOLISM	0.011235955	0.1558389
KEGG_INTESTINAL_IMMUNE_NETWORK_FOR_IGA_PRODUCTION	0.03141361	0.16073199
KEGG_ABC_TRANSPORTERS	0.01038961	0.16581017
KEGG_OXIDATIVE_PHOSPHORYLATION	0.003333333	0.178059
KEGG_PROPANOATE_METABOLISM	0.046035804	0.22476496
KEGG_PEROXISOME	0.026865672	0.2373898

B

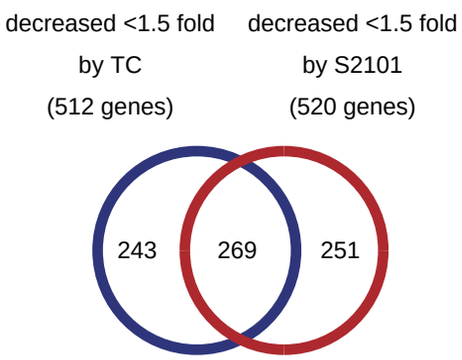

downregulated by LSD1 inhibition

NAME	NOM p-value	FDR q-value
KEGG_CELL_CYCLE	<0.001	0.004345598
KEGG_DNA_REPLICATION	0.001618123	0.021393025
KEGG_MISMATCH_REPAIR	0.026086956	0.23018923
KEGG_FOCAL_ADHESION	0.007032349	0.2200881
KEGG_ECM_RECEPTOR_INTERACTION	0.015360983	0.21840344

Anan *et al.* Figure S2

A

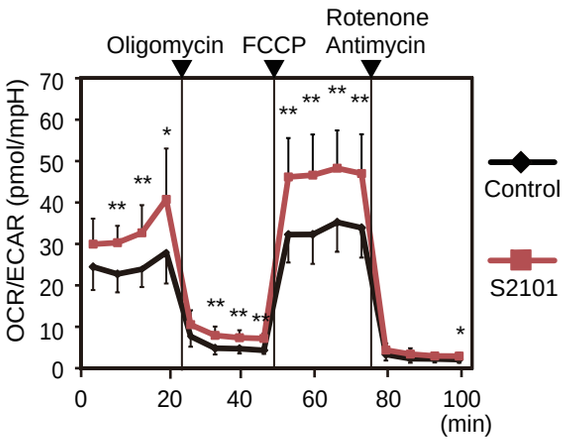

B

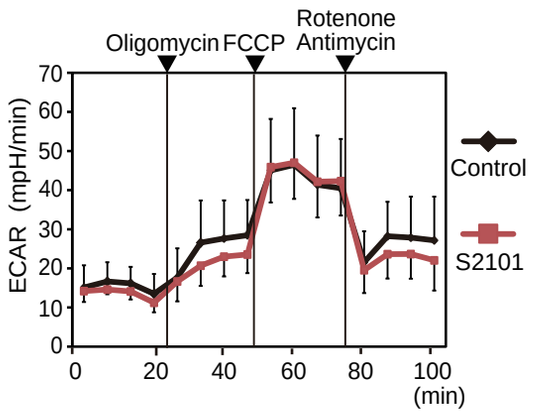

C

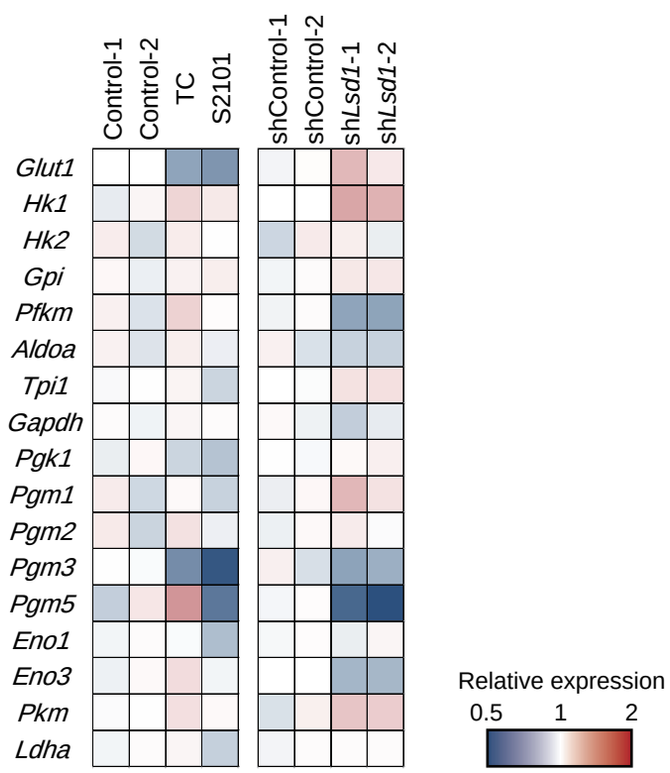

Anan *et al.* Figure S3

A

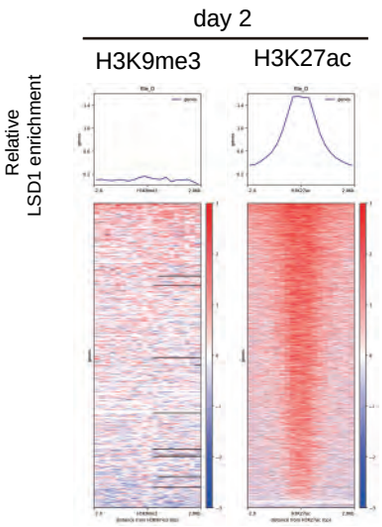

B

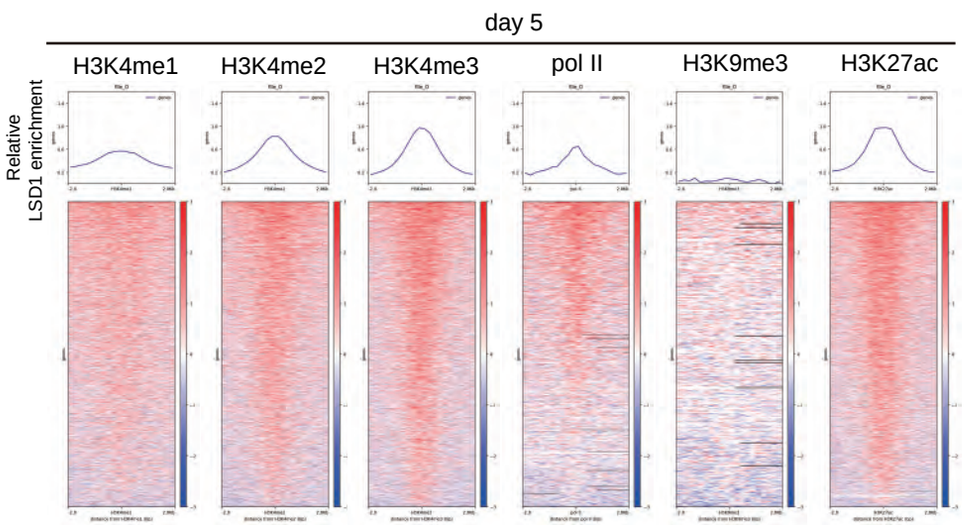

Anan *et al.* Figure S4

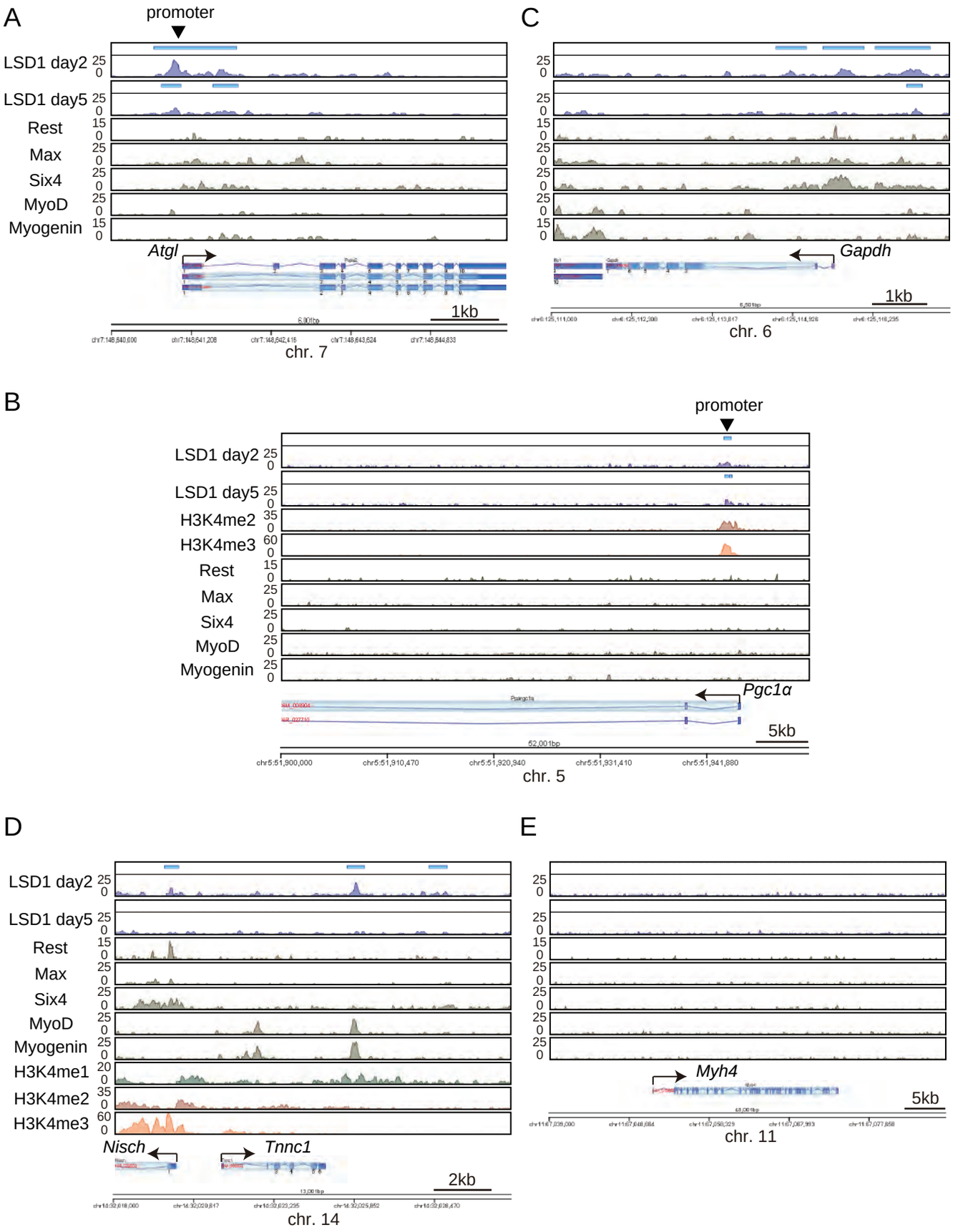

Anan *et al.* Figure S5

A

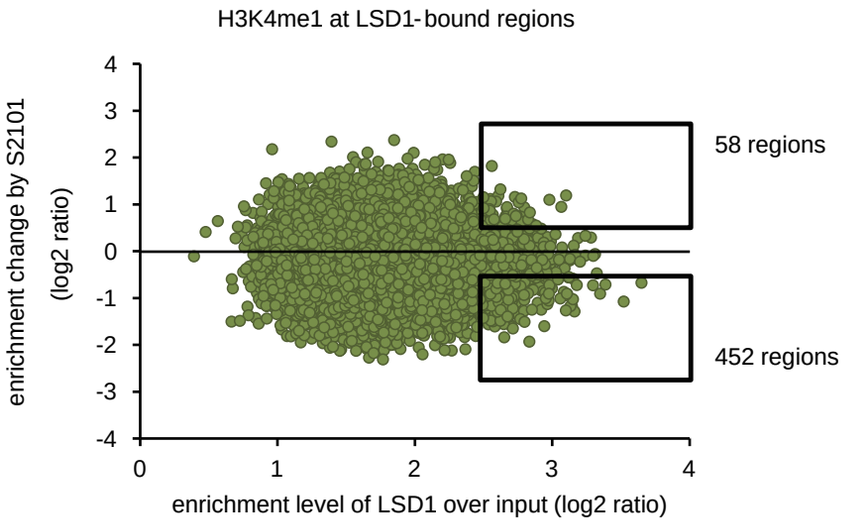

B

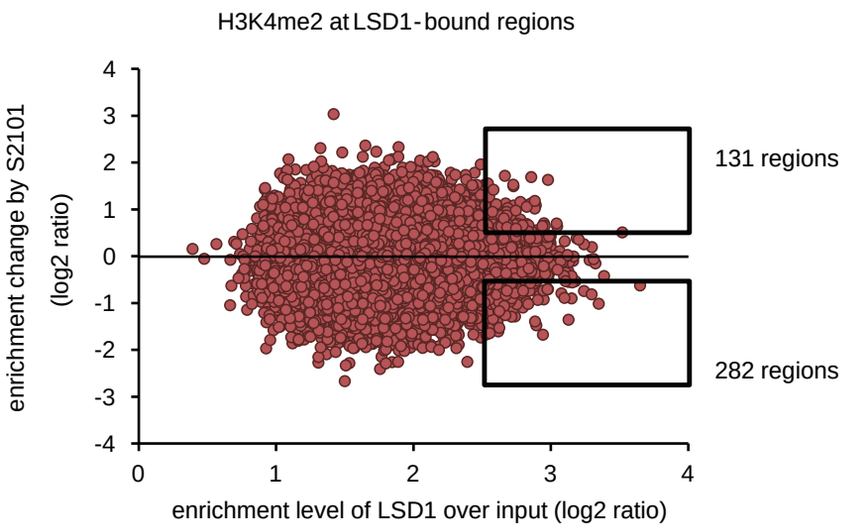

C

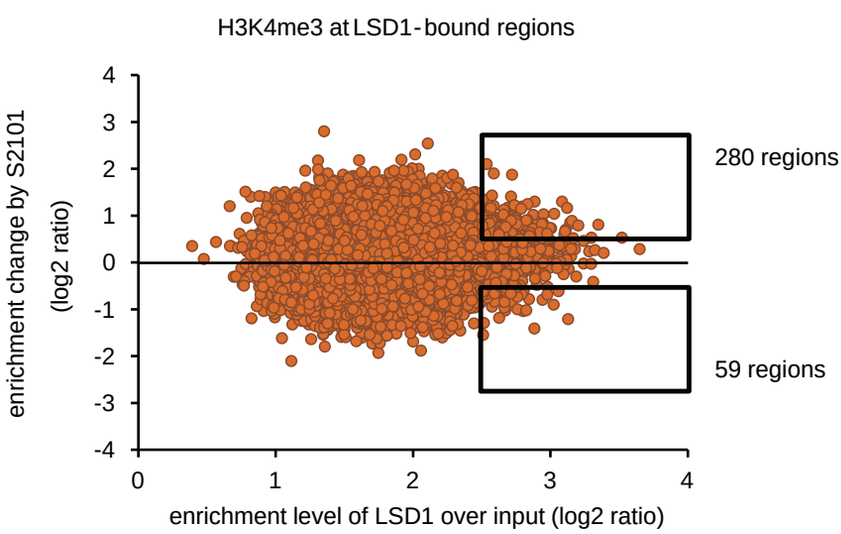

Anan *et al.* Figure S6

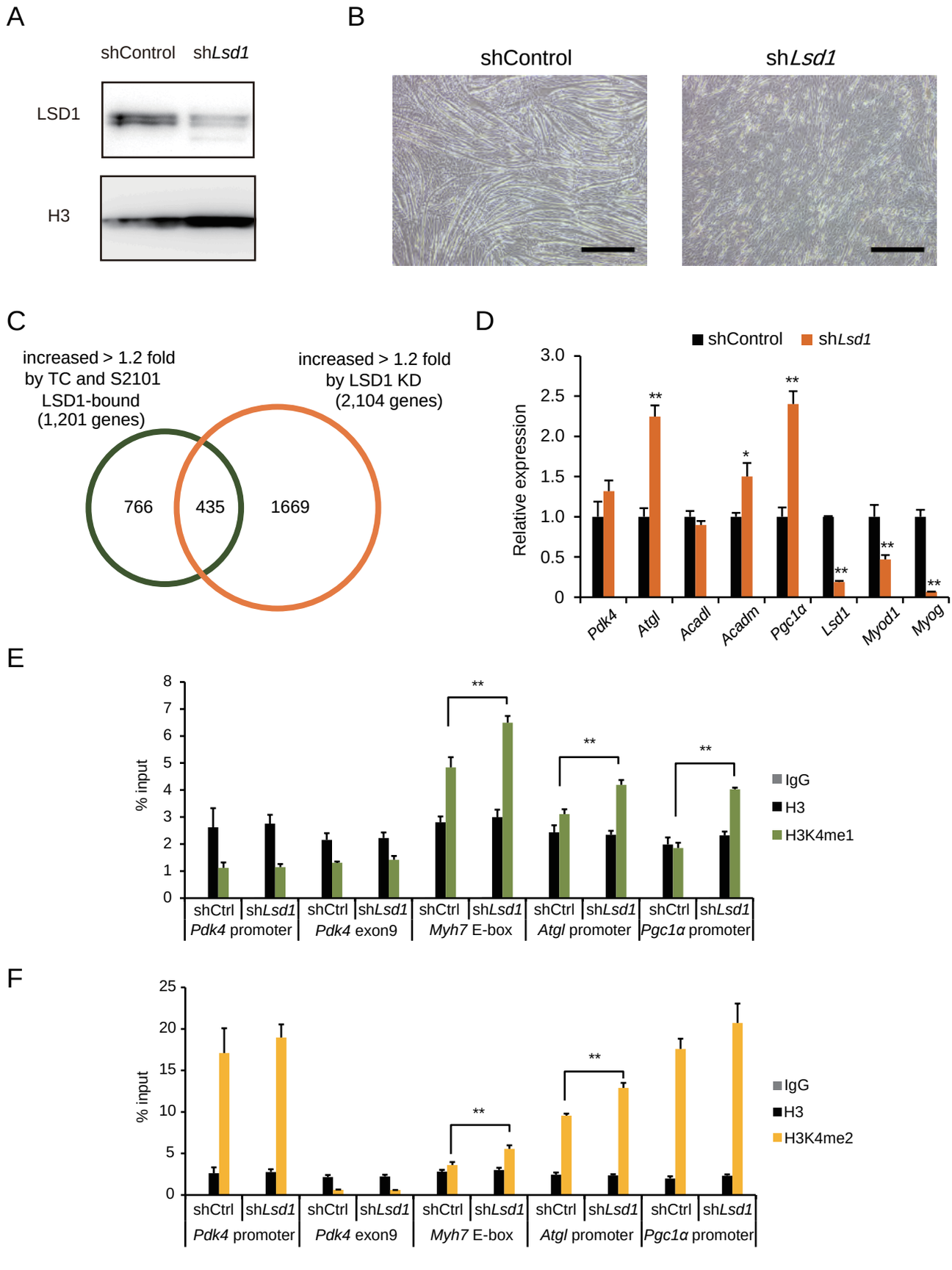

Anan *et al.* Figure S7

A

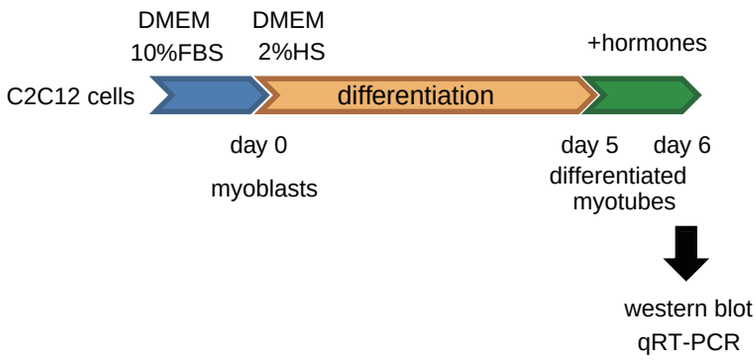

B

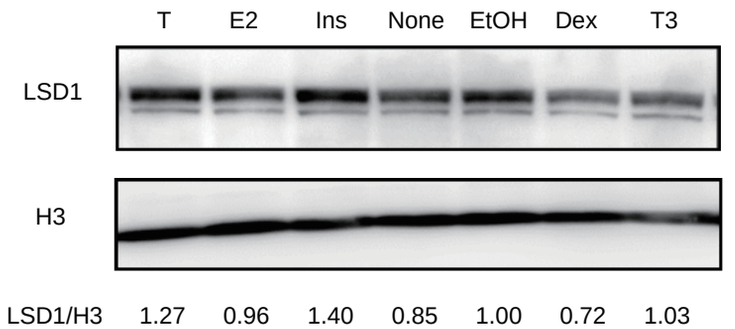

C

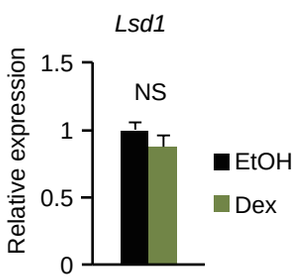

D

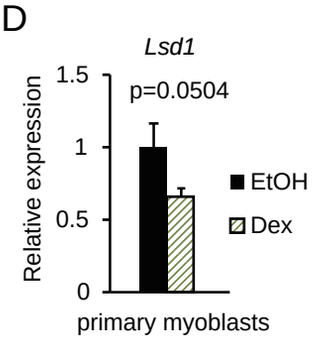

Anan *et al.* Figure S8

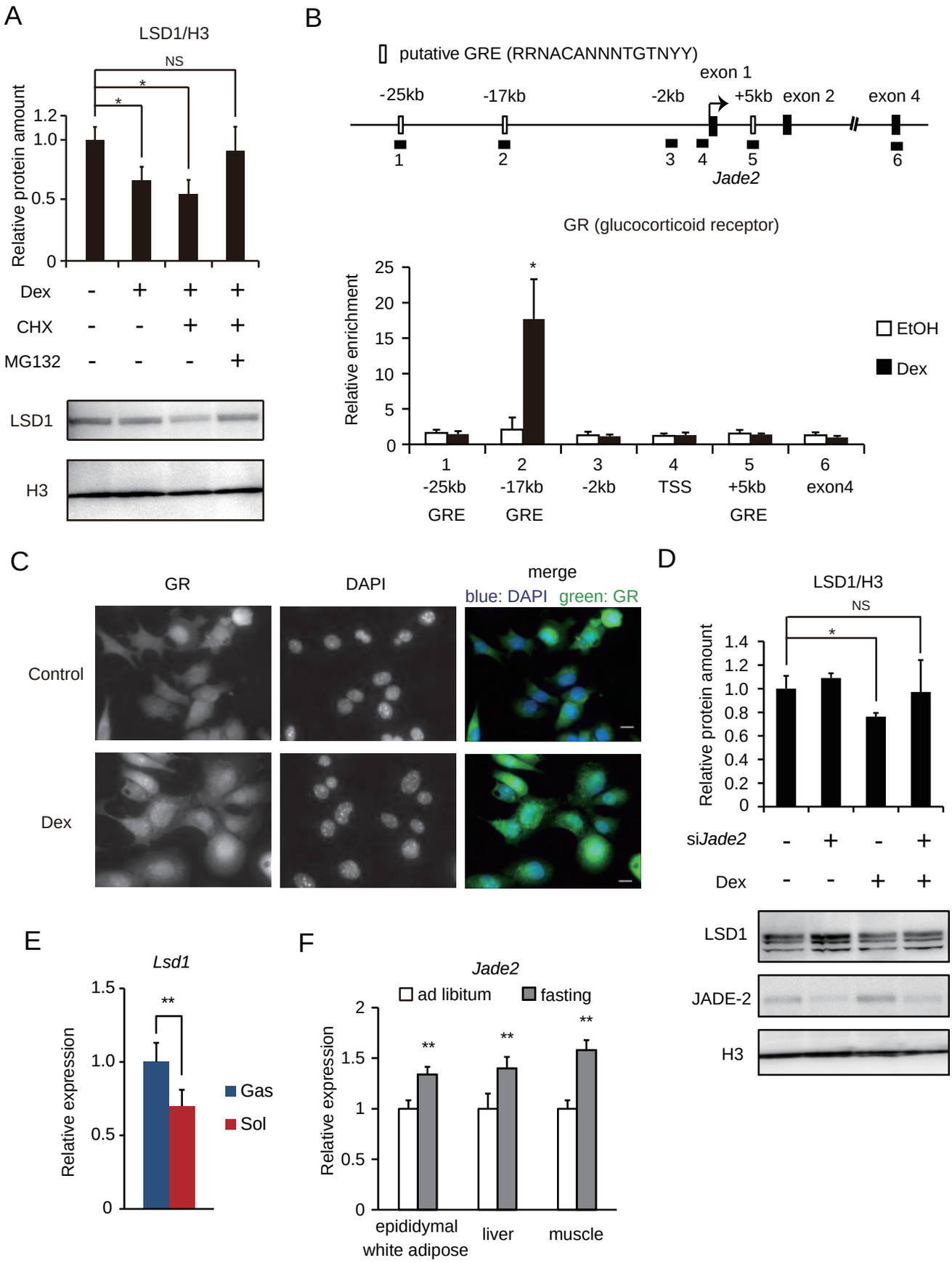

Anan *et al.* Figure S9

A

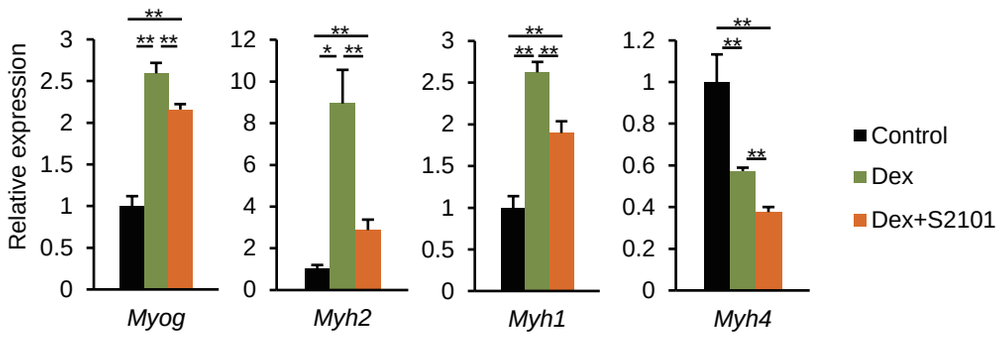

B

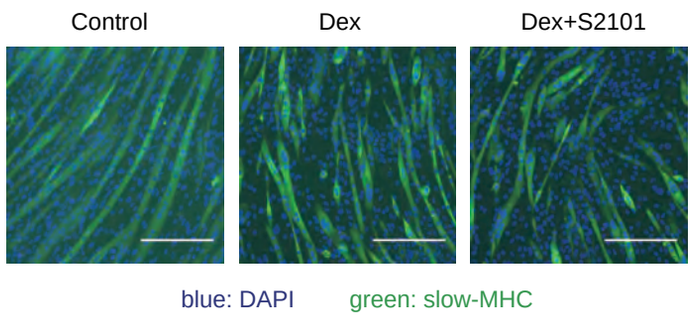

C

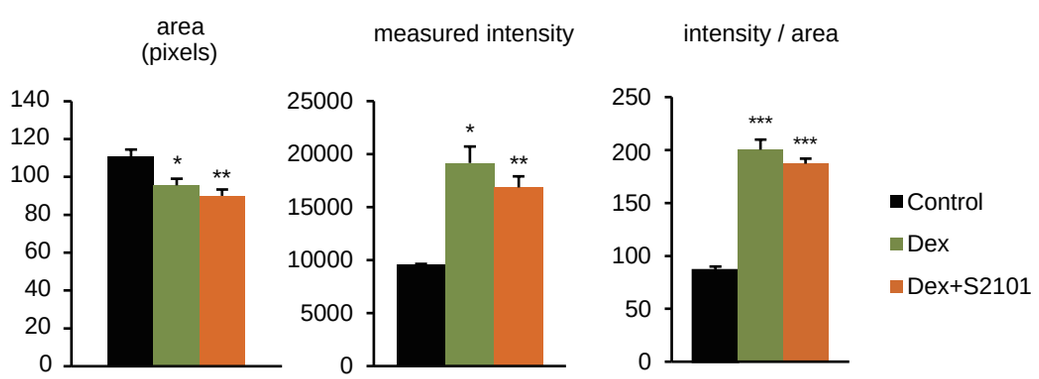

Anan *et al.* Figure S10

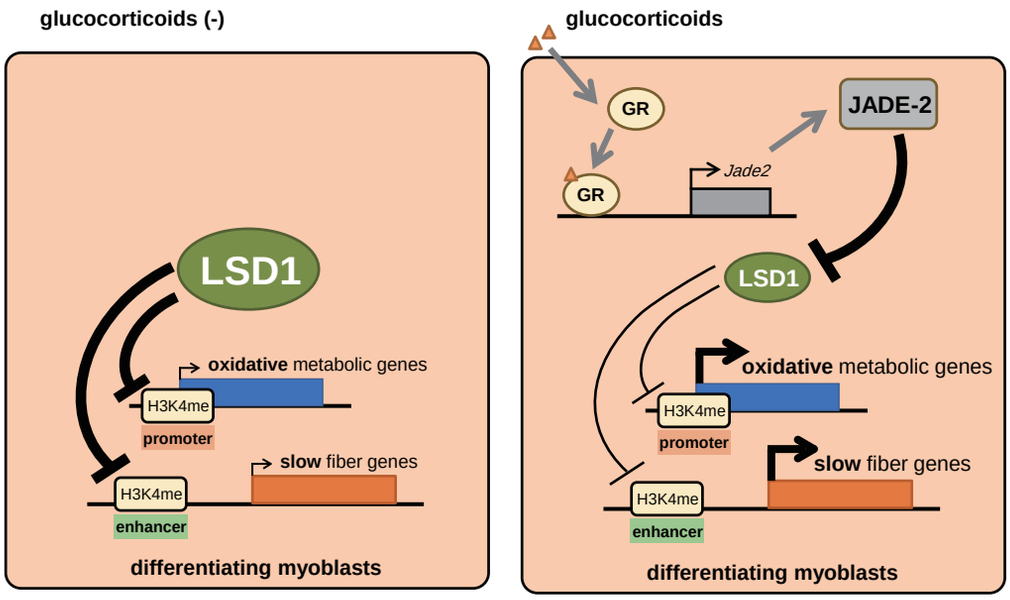

Anan *et al.* Figure S11

Figure 4A

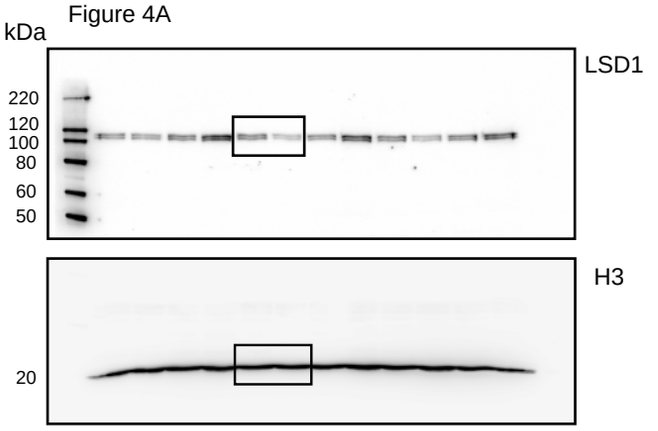

Figure 4B

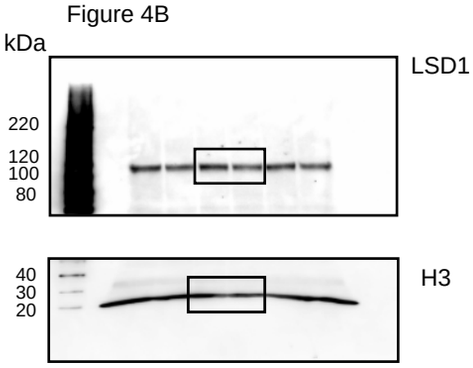

Figure 4D

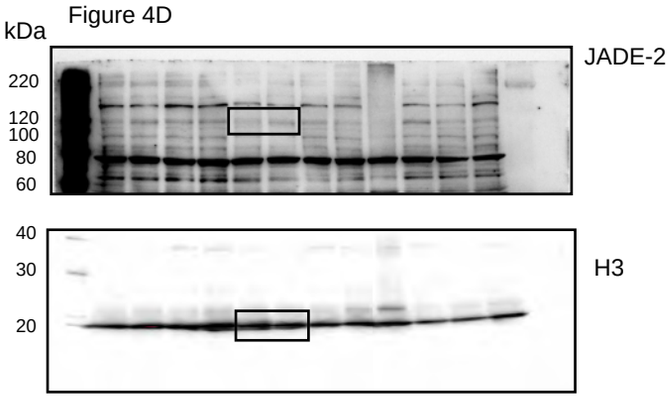

Figure 4F

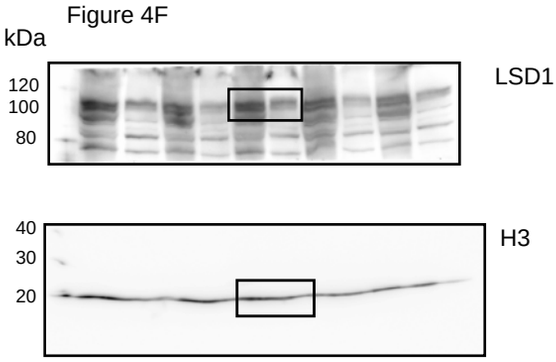

Figure 4G

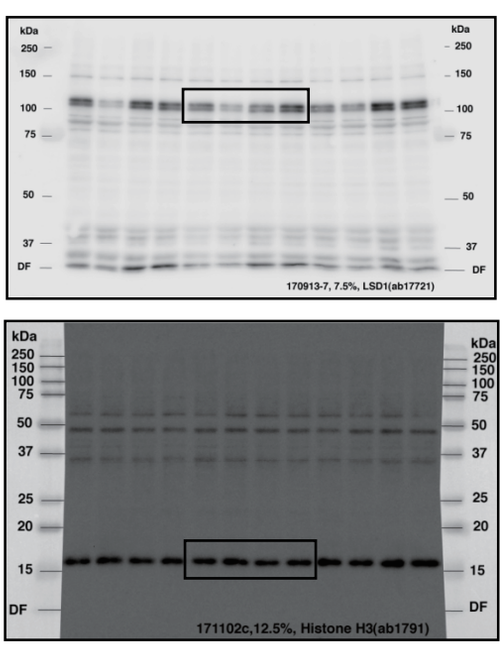

Figure 4I

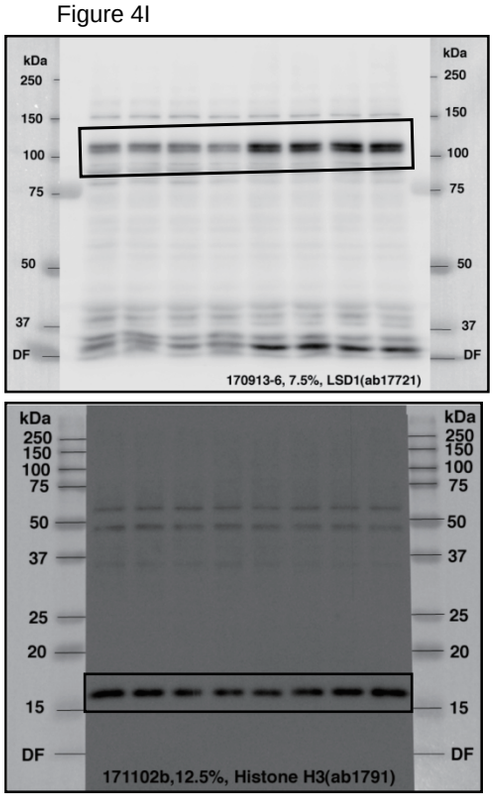

Figure S7A

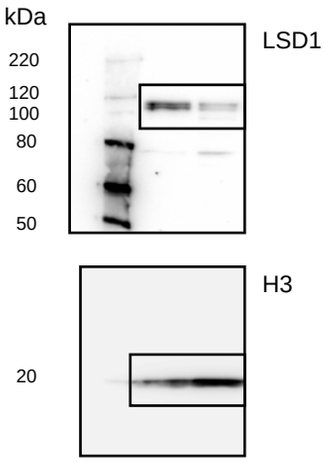

Figure S8B

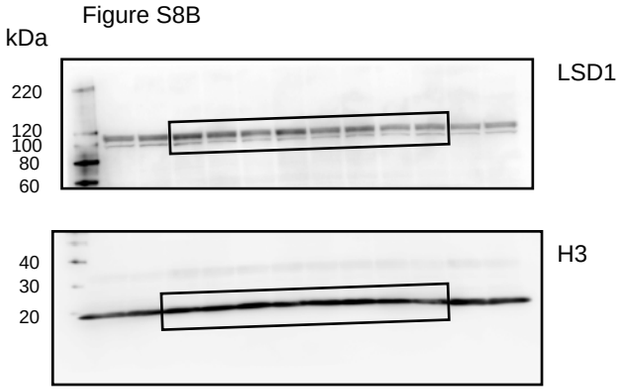

Figure S9A

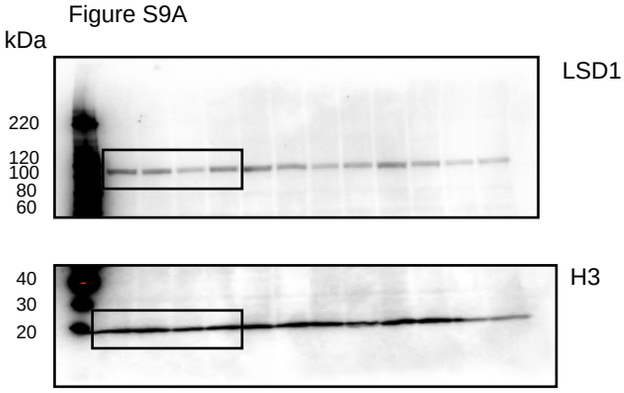

Figure S9D

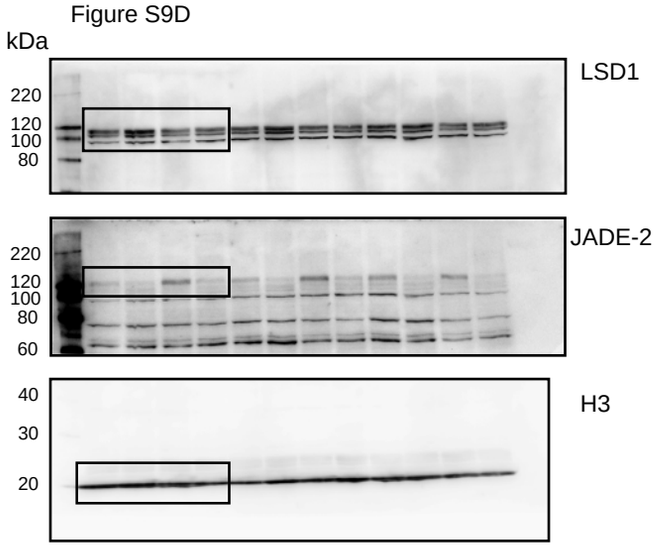

Table S1 - Primers used in this study

Gene Symbol	Gene Name	Forward (5'-3')	Reverse (5'-3')
Quantitative RT-PCR			
36B4	ribosomal protein, large, P0	GCGTCCTGGCATTGTCTGT	GCAAATGCAGATGGATCAGCC
Lsd1	lysine (K)-specific demethylase 1A	ATGGATGTCACACTTCTGGA	CAAGACCTGTTACAACCATG
Pdk4	pyruvate dehydrogenase kinase, isoenzyme 4	CAAGGAGATCTGAATCTCTA	GATAATGTTTGAAGGCTGAC
Atgl	adipose triglyceride lipase (patatin-like phospholipase domain containing 2)	GCCAACGCCACTCACATCTA	GCCTCCTTGGACACCTCAAT
Acadl	acyl-Coenzyme A dehydrogenase, long-chain	AGAACAGATCGAGAAGTTCA	GCGTTCGTTCTTACTCCTTG
Acadm	acyl-Coenzyme A dehydrogenase, medium chain	ATTTGGAAAGCTGCTAGTGG	TGGTAACTGAGCCTAGCGAG
Pgc1α	peroxisome proliferative activated receptor, gamma, coactivator 1 alpha	AAGTGTGGAACTCTCTGGAACTG	GGGTTATCTTGGTTGGCTTTATG
Myh7	myosin, heavy polypeptide 7, cardiac muscle, beta	CTCAAGCTGCTCAGCAATCTATTT	GGAGCGCAAGTTTGTCATAAGT
Myh2	myosin, heavy polypeptide 2, skeletal muscle, adult	GAGCAAAGATGCAGGGAAAG	TAAGGGTTGACGGTGACACA
Myh1	myosin, heavy polypeptide 1, skeletal muscle, adult	GCATCGAGTGGGAGTTCATT	TGAGCTTCAACCTTGCCTTT
Myh4	myosin, heavy polypeptide 4, skeletal muscle	ACATTATTGGCTGGCTGGAC	ACCCTTCTTCTTGCCACCTT
Myl2	myosin, light polypeptide 2, regulatory, cardiac, slow	TGACCACACAAGCAGAGAGG	CCGTGGGTAATGATGTGGA
Myl1	myosin, light polypeptide 1	CCCAGCCAAACCTAAGGAAG	TGCATTCACCTGTTCTGTCAA
Mylpf	myosin light chain, phosphorylatable, fast skeletal muscle	AGGGAGCTCCAACGTCTTCT	GCGTCGAGTTCCTCATTCTT
Jade1	jade family PHD finger 1	CCCAGCAGCAGTGAGGATT	GATCAGGTCGGTCCTAAACA
Jade2	jade family PHD finger 2	CCATCAGCAGCGACAACTCT	TGAGGGCTTCTTCTCGTTCT
Usp28	ubiquitin specific peptidase 28	GAGCTGCAGCAGGACGACT	ATCCTGGATGCCTGTGATTT
Myod1	myogenic differentiation 1	TACAGTGGCGACTCAGATGC	GAGATGCGCTCCACTATGCT
Myog	myogenin	CAGTGAATGCAACTCCCACAGC	CACCCAGCCTGACAGACAATCTC
ChIP-quantitative PCR			
Pdk4	promoter	CTGGCTAGGAATGCGTGACA	GATCCCAGGTCGCTAGGACT
	exon 9	GGTGTTCCTCTGAGGATTAC	GCATTCCGGGAATTGTCCAT
Atgl	promoter	TGCCCAAGCTGTGGGATTGA	AGCCATCTGAGAGACCTGGA
Pgc1α	promoter	GAGCAGCTCACTGCTTGTGT	CTCCAGAGATTACGGGGAAA
	+100kb	CACAAACACCTGGCACTCAC	CCACTTGCCTCATGCTGACA
Myh7	E-box	GGGTGCCTGGTGTATTGAGT	GCCAGGATTAGGGAGCTGA
	promoter	GGGGGAAATGCTTTTAGTGA	CAGCTCCCACTCCTACCTGA
	exon 4	GCGGGAAGGCATATAGGTAA	CATCGGGCACAAAAACATC
	+10kb	CCACAATCCCACACCTCTCT	ATGCCTGAGCCTGCGTATTT
Jade2	1	CAAGCCATAGAGACACCCAAC	CAGTGGAGTGAAGGGAGAACA
	2	TGTGTCTGTGGCTGGATGA	CGGCTCTCTGTTTCCAGATT
	3	TGGAGGGGAAAGGAAAAATAA	TTTTTGAAGGCAGGTGGATG
	4	CATCGCAGTTGGAGGCTATT	CCTGCTGGGAAGATGGTC
	5	GGATGGGACAGCTCATTTCT	AGGTTTTTCCTGCTTCCACA
	6	TCCCAGATTCATACCAGCTCA	CACCCCTTTCTCCCATTCTT

Table S2 - Mapped read counts in ChIP-seq analysis

Experiment #	Cells	Condition	Antigen	Read counts
1	C2C12	normally differentiated, on day 2	input	16472156
1	C2C12	normally differentiated, on day 2	LSD1	18031920
2	C2C12	normally differentiated, on day 5	input	17298668
2	C2C12	normally differentiated, on day 5	LSD1	15778509
3	C2C12	differentiated with control vehicle, on day 2	input	15068639
3	C2C12	differentiated with control vehicle, on day 2	H3K4me1	17664635
3	C2C12	differentiated with control vehicle, on day 2	H3K4me2	13126558
3	C2C12	differentiated with S2101, on day 2	input	13267750
3	C2C12	differentiated with S2101, on day 2	H3K4me1	10139301
3	C2C12	differentiated with S2101, on day 2	H3K4me2	12139283
4	C2C12	differentiated with control vehicle, on day 2	input	14798951
4	C2C12	differentiated with control vehicle, on day 2	H3	19367010
4	C2C12	differentiated with control vehicle, on day 2	H3K4me3	13074866
4	C2C12	differentiated with S2101, on day 2	input	17021862
4	C2C12	differentiated with S2101, on day 2	H3	15851644
4	C2C12	differentiated with S2101, on day 2	H3K4me3	14256097

Table S3 - 435 LSD1-bound genes upregulated by both inhibitors and LSD1 KD

Gene Symbol	Gene Title
0610010O12Rik	RIKEN cDNA 0610010O12 gene
1200009I06Rik	RIKEN cDNA 1200009I06 gene
1700052N19Rik	RIKEN cDNA 1700052N19 gene
1700112E06Rik	RIKEN cDNA 1700112E06 gene
1810012P15Rik	RIKEN cDNA 1810012P15 gene
1810013D10Rik	RIKEN cDNA 1810013D10 gene
1810014F10Rik	RIKEN cDNA 1810014F10 gene
2310044G17Rik	RIKEN cDNA 2310044G17 gene
2410066E13Rik	RIKEN cDNA 2410066E13 gene
2410076I21Rik	RIKEN cDNA 2410076I21 gene
A930001N09Rik	RIKEN cDNA A930001N09 gene
AA467197	expressed sequence AA467197
Abca2	ATP-binding cassette, sub-family A (ABC1), member 2
Abca3	ATP-binding cassette, sub-family A (ABC1), member 3
Abcd2	ATP-binding cassette, sub-family D (ALD), member 2
Acer3	alkaline ceramidase 3
Acot11	acyl-CoA thioesterase 11
Acss2	acyl-CoA synthetase short-chain family member 2
Adamtsl1	ADAMTS-like 1
Adamtsl4	ADAMTS-like 4
Adamtsl5	ADAMTS-like 5
Adh7	alcohol dehydrogenase 7 (class IV), mu or sigma polypeptide
Adi1	acireductone dioxygenase 1
Adora2b	adenosine A2b receptor
Afap1l2	actin filament associated protein 1-like 2
Aig1	androgen-induced 1
Aldh1l1	aldehyde dehydrogenase 1 family, member L1
Aldh2	aldehyde dehydrogenase 2, mitochondrial
Aldh3a1	aldehyde dehydrogenase family 3, subfamily A1
Aldoc	aldolase C, fructose-bisphosphate
Ampd3	adenosine monophosphate deaminase 3
Aox1	aldehyde oxidase 1
Ap1g2	adaptor protein complex AP-1, gamma 2 subunit
Apobec1	apolipoprotein B mRNA editing enzyme, catalytic polypeptide 1
Apol7a	apolipoprotein L 7a
Aqp1	aquaporin 1
Aqp5	aquaporin 5
Ar	androgen receptor
Areg	amphiregulin
Arhgap18	Rho GTPase activating protein 18
Arhgef3	Rho guanine nucleotide exchange factor (GEF) 3
Armc10	armadillo repeat containing 10
Arrb2	arrestin, beta 2
Artn	artemin
Arvcf	armadillo repeat gene deleted in velo-cardio-facial syndrome
As3mt	arsenic (+3 oxidation state) methyltransferase
Asl	argininosuccinate lyase
Atat1	alpha tubulin acetyltransferase 1
Atl1	atlastin GTPase 1
Atl3	atlastin GTPase 3
Atp6v0e2	ATPase, H+ transporting, lysosomal V0 subunit E2
AU018091	expressed sequence AU018091
Axl	AXL receptor tyrosine kinase
BC046404	cDNA sequence BC046404
BC052040	cDNA sequence BC052040
Bdh2	3-hydroxybutyrate dehydrogenase, type 2
Bdkrb2	bradykinin receptor, beta 2
Best1	bestrophin 1
Bicd1	bicaudal D homolog 1 (Drosophila)

Bid	BH3 interacting domain death agonist
Bik	BCL2-interacting killer
Blnk	B cell linker
Bst2	bone marrow stromal cell antigen 2
Btbd11	BTB (POZ) domain containing 11
C1galt1	core 1 synthase, glycoprotein-N-acetylgalactosamine 3-beta-galactosyltransferase, 1
C1s	complement component 1, s subcomponent
C630004H02Rik	RIKEN cDNA C630004H02 gene
Cacfd1	calcium channel flower domain containing 1
Cacnb2	calcium channel, voltage-dependent, beta 2 subunit
Cadm4	cell adhesion molecule 4
Calcrl	calcitonin receptor-like
Capn5	calpain 5
Car13	carbonic anhydrase 13
Car2	carbonic anhydrase 2
Car3	carbonic anhydrase 3
Car7	carbonic anhydrase 7
Car8	carbonic anhydrase 8
Card10	caspase recruitment domain family, member 10
Cbr2	carbonyl reductase 2
Cck	cholecystokinin
Cd24a	CD24a antigen
Cd55	CD55 antigen
Cda	cytidine deaminase
Cdc42bpg	CDC42 binding protein kinase gamma (DMPK-like)
Cdh1	cadherin 1
Cdk2ap2	CDK2-associated protein 2
Cebpb	CCAAT/enhancer binding protein (C/EBP), beta
Celf5	CUGBP, Elav-like family member 5
Cerk	ceramide kinase
Cgnl1	cingulin-like 1
Ch25h	cholesterol 25-hydroxylase
Chchd10	coiled-coil-helix-coiled-coil-helix domain containing 10
Chd7	chromodomain helicase DNA binding protein 7
Chd8	chromodomain helicase DNA binding protein 8
Chek1	checkpoint kinase 1
Chmp4c	charged multivesicular body protein 4C
Chn2	chimerin (chimaerin) 2
Cklf	chemokine-like factor
Clca5	chloride channel calcium activated 5
Clcn3	chloride channel 3
Cldn7	claudin 7
Cldn9	claudin 9
Clic5	chloride intracellular channel 5
Clip4	CAP-GLY domain containing linker protein family, member 4
Clmn	calmin
Clu	clusterin
Cmbl	carboxymethylenebutenolidase-like (Pseudomonas)
Cobl	cordon-bleu
Cobll1	Cobl-like 1
Coro1a	coronin, actin binding protein 1A
Cox7a1	cytochrome c oxidase, subunit VIIa 1
Cpd	carboxypeptidase D
Creb5	cAMP responsive element binding protein 5
Creld1	cysteine-rich with EGF-like domains 1
Crem	cAMP responsive element modulator
Csf2rb	colony stimulating factor 2 receptor, beta, low-affinity (granulocyte-macrophage)
Cst6	cystatin E/M
Ctnnal1	catenin (cadherin associated protein), alpha-like 1
Ctsb	cathepsin B
Cxcr4	chemokine (C-X-C motif) receptor 4

Cyfip2	cytoplasmic FMR1 interacting protein 2
Cyp26a1	cytochrome P450, family 26, subfamily a, polypeptide 1
Dab2	disabled 2, mitogen-responsive phosphoprotein
Dact2	dapper homolog 2, antagonist of beta-catenin (xenopus)
Dbi	diazepam binding inhibitor
Ddah1	dimethylarginine dimethylaminohydrolase 1
Dennd3	DENN/MADD domain containing 3
Dmxl2	Dmx-like 2
Dntt	Deoxynucleotidyltransferase, terminal
Dock11	dedicator of cytokinesis 11
Dock5	dedicator of cytokinesis 5
Dock8	dedicator of cytokinesis 8
Dock9	dedicator of cytokinesis 9
Dok7	docking protein 7
Dopey2	dopey family member 2
Dpp7	dipeptidylpeptidase 7
Dpy19l3	dpy-19-like 3 (C. elegans)
Dtd1	D-tyrosyl-tRNA deacylase 1 homolog (S. cerevisiae)
Dtna	dystrobrevin alpha
Dtwd2	DTW domain containing 2
E130308A19Rik	RIKEN cDNA E130308A19 gene
Elovl6	ELOVL family member 6, elongation of long chain fatty acids (yeast)
Elovl7	ELOVL family member 7, elongation of long chain fatty acids (yeast)
Eml2	echinoderm microtubule associated protein like 2
Eml5	echinoderm microtubule associated protein like 5
Enpp4	ectonucleotide pyrophosphatase/phosphodiesterase 4
Epb4.1l5	erythrocyte protein band 4.1-like 5
Epb4.9	erythrocyte protein band 4.9
Ephx4	epoxide hydrolase 4
Epn2	epsin 2
Eps8	epidermal growth factor receptor pathway substrate 8
Ermp1	endoplasmic reticulum metallopeptidase 1
Etfdh	electron transferring flavoprotein, dehydrogenase
Ethe1	ethylmalonic encephalopathy 1
Etl4	enhancer trap locus 4
Exd1	exonuclease 3'-5' domain containing 1
Exoc6	exocyst complex component 6
Eya1	eyes absent 1 homolog (Drosophila)
Ezr	ezrin
F11r	F11 receptor
Fads2	fatty acid desaturase 2
Fam107a	family with sequence similarity 107, member A
Fam55c	family with sequence similarity 55, member C
Fam84b	family with sequence similarity 84, member B
Fdft1	farnesyl diphosphate farnesyl transferase 1
Fetub	fetuin beta
Fez1	fasciculation and elongation protein zeta 1 (zygin I)
Fgd2	FYVE, RhoGEF and PH domain containing 2
Fgl2	fibrinogen-like protein 2
Foxc2	forkhead box C2
Foxred2	FAD-dependent oxidoreductase domain containing 2
Galm	galactose mutarotase
Galnt6	UDP-N-acetyl-alpha-D-galactosamine:polypeptide N-acetylgalactosaminyltransferase 6
Galnt7	UDP-N-acetyl-alpha-D-galactosamine: polypeptide N-acetylgalactosaminyltransferase 7
Gbe1	glucan (1,4-alpha-), branching enzyme 1
Gch1	GTP cyclohydrolase 1
Gcnt2	glucosaminyl (N-acetyl) transferase 2, I-branching enzyme
Gdpd1	glycerophosphodiester phosphodiesterase domain containing 1
Gdpd5	glycerophosphodiester phosphodiesterase domain containing 5
Gfra2	glial cell line derived neurotrophic factor family receptor alpha 2
Gja3	gap junction protein, alpha 3

Gm2a	GM2 ganglioside activator protein
Gna14	guanine nucleotide binding protein, alpha 14
Gpm6b	glycoprotein m6b
Gpnmb	glycoprotein (transmembrane) nmb
Gpr133	G protein-coupled receptor 133
Gpr173	G-protein coupled receptor 173
Gramd1b	GRAM domain containing 1B
Grasp	GRP1 (general receptor for phosphoinositides 1)-associated scaffold protein
Grina	glutamate receptor, ionotropic, N-methyl D-aspartate-associated protein 1 (glutamate binding)
Grn	granulin
Gspt2	G1 to S phase transition 2
Gsta4	glutathione S-transferase, alpha 4
Gstm1	glutathione S-transferase, mu 1
Havcr2	hepatitis A virus cellular receptor 2
Hdc	histidine decarboxylase
Heg1	HEG homolog 1 (zebrafish)
Hltf	helicase-like transcription factor
Hnmt	histamine N-methyltransferase
Hoxa3	homeobox A3
Hsd3b7	hydroxy-delta-5-steroid dehydrogenase, 3 beta- and steroid delta-isomerase 7
Hspa4l	heat shock protein 4 like
Htr1b	5-hydroxytryptamine (serotonin) receptor 1B
Id2	inhibitor of DNA binding 2
Ier3	immediate early response 3
Ifitm1	interferon induced transmembrane protein 1
Ifitm3	interferon induced transmembrane protein 3
Igfbp5	insulin-like growth factor binding protein 5
Il33	interleukin 33
Il6ra	interleukin 6 receptor, alpha
Insig1	insulin induced gene 1
Insl6	insulin-like 6
Irgm2	immunity-related GTPase family M member 2
Itgb8	integrin beta 8
Itgbl1	integrin, beta-like 1
Kat2b	K(lysine) acetyltransferase 2B
Kbtbd11	kelch repeat and BTB (POZ) domain containing 11
Kcnab3	potassium voltage-gated channel, shaker-related subfamily, beta member 3
Kcnmb2	potassium large conductance calcium-activated channel, subfamily M, beta member 2
Kif13b	kinesin family member 13B
Kif16b	kinesin family member 16B
Kif21a	kinesin family member 21A
Krt80	keratin 80
Lama3	laminin, alpha 3
Lama5	laminin, alpha 5
Lims2	LIM and senescent cell antigen like domains 2
Lmbr1	limb region 1
Lonrf3	LON peptidase N-terminal domain and ring finger 3
Lrba	LPS-responsive beige-like anchor
Lrrc27	leucine rich repeat containing 27
Lrrc8b	leucine rich repeat containing 8 family, member B
Lrrc8d	leucine rich repeat containing 8D
Lrsam1	leucine rich repeat and sterile alpha motif containing 1
Lztr1	leucine-zipper-like transcriptional regulator, 1
Magi3	membrane associated guanylate kinase, WW and PDZ domain containing 3
Manba	mannosidase, beta A, lysosomal
Map1lc3a	microtubule-associated protein 1 light chain 3 alpha
Map3k8	mitogen-activated protein kinase kinase kinase 8
Map4k2	mitogen-activated protein kinase kinase kinase kinase 2
Mapre2	microtubule-associated protein, RP/EB family, member 2
Mapt	microtubule-associated protein tau
Mblac2	metallo-beta-lactamase domain containing 2

Mfap3l	microfibrillar-associated protein 3-like
Mfsd6	major facilitator superfamily domain containing 6
Mical3	microtubule associated monoxygenase, calponin and LIM domain containing 3
Mknk2	MAP kinase-interacting serine/threonine kinase 2
Mkrn1	makorin, ring finger protein, 1
Mt2	metallothionein 2
Mtap2	microtubule-associated protein 2
Mtch2	mitochondrial carrier homolog 2 (C. elegans)
Mtss1	metastasis suppressor 1
Naip2	NLR family, apoptosis inhibitory protein 2
Nalcn	sodium leak channel, non-selective
Nbeal2	neurobeachin-like 2
Ncald	neurocalcin delta
Nceh1	arylacetamide deacetylase-like 1
Ndrg2	N-myc downstream regulated gene 2
Ndrg4	N-myc downstream regulated gene 4
Nebl	nebulette
Nedd9	neural precursor cell expressed, developmentally down-regulated gene 9
Neu1	neuraminidase 1
Nfe2l2	nuclear factor, erythroid derived 2, like 2
Nipal3	NIPA-like domain containing 3
Nkd2	naked cuticle 2 homolog (Drosophila)
Nlrc5	NLR family, CARD domain containing 5
Nqo1	NAD(P)H dehydrogenase, quinone 1
Nrn1	neuritin 1
Nrxn3	neurexin III
Nsg1	neuron specific gene family member 1
Nt5e	5' nucleotidase, ecto
Nup210	nucleoporin 210
Obfc2a	oligonucleotide/oligosaccharide-binding fold containing 2A
Ociad2	OCIA domain containing 2
Ocln	occludin
Odz4	odd Oz/ten-m homolog 4 (Drosophila)
Olfm1	olfactomedin 1
Pag1	phosphoprotein associated with glycosphingolipid microdomains 1
Pcbd1	pterin 4 alpha carbinolamine dehydratase/dimerization cofactor of hepatocyte nuclear factor 1 alpha (TCF1) 1
Pcp4l1	Purkinje cell protein 4-like 1
Pde4b	phosphodiesterase 4B, cAMP specific
Pde4dip	phosphodiesterase 4D interacting protein (myomegalin)
Pdk4	pyruvate dehydrogenase kinase, isoenzyme 4
Peg3	paternally expressed 3
Perp	PERP, TP53 apoptosis effector
Pgpep1	pyroglutamyl-peptidase I
Pi15	peptidase inhibitor 15
Pik3ip1	phosphoinositide-3-kinase interacting protein 1
Pim1	proviral integration site 1
Pkp2	Plakophilin 2
Pla2g2e	phospholipase A2, group IIE
Pla2g6	phospholipase A2, group VI
Plcg2	phospholipase C, gamma 2
Plcl2	phospholipase C-like 2
Plekha6	pleckstrin homology domain containing, family A member 6
Plekha7	pleckstrin homology domain containing, family A member 7
Plekhb1	pleckstrin homology domain containing, family B (evectins) member 1
Plin2	perilipin 2
Pltp	phospholipid transfer protein
Plxdc1	plexin domain containing 1
Plxdc2	plexin domain containing 2
Pmvk	phosphomevalonate kinase
Pnpla2	patatin-like phospholipase domain containing 2

Pnpla6	patatin-like phospholipase domain containing 6
Podxl	podocalyxin-like
Pou4f1	POU domain, class 4, transcription factor 1
Ppp1r9a	protein phosphatase 1, regulatory (inhibitor) subunit 9A
Prkag2	protein kinase, AMP-activated, gamma 2 non-catalytic subunit
Prrg4	proline rich Gla (G-carboxyglutamic acid) 4 (transmembrane)
Prrx1	paired related homeobox 1
Psca	prostate stem cell antigen
Ptgds	prostaglandin D2 synthase (brain)
Ptgis	prostaglandin I2 (prostacyclin) synthase
Ptgs1	prostaglandin-endoperoxide synthase 1
Ptp4a3	protein tyrosine phosphatase 4a3
Ptplb	protein tyrosine phosphatase-like (proline instead of catalytic arginine), member b
Ptpn22	protein tyrosine phosphatase, non-receptor type 22 (lymphoid)
Qpct	glutaminyl-peptide cyclotransferase (glutaminyl cyclase)
Qser1	glutamine and serine rich 1
Rab20	RAB20, member RAS oncogene family
Rab27b	RAB27b, member RAS oncogene family
Rab3il1	RAB3A interacting protein (rabin3)-like 1
Rab3ip	RAB3A interacting protein
Rab43	RAB43, member RAS oncogene family
Rabepk	Rab9 effector protein with kelch motifs
Ralb	v-ral simian leukemia viral oncogene homolog B (ras related)
Ralgapa1	Ral GTPase activating protein, alpha subunit 1
Ralgps1	Ral GEF with PH domain and SH3 binding motif 1
Ralgps2	Ral GEF with PH domain and SH3 binding motif 2
Rapgef3	Rap guanine nucleotide exchange factor (GEF) 3
Rarb	retinoic acid receptor, beta
Rasa3	RAS p21 protein activator 3
Rassf2	Ras association (RalGDS/AF-6) domain family member 2
Rassf4	Ras association (RalGDS/AF-6) domain family member 4
Rbm47	RNA binding motif protein 47
Rcan3	regulator of calcineurin 3
Reep2	receptor accessory protein 2
Repin1	replication initiator 1
Rftn1	raftlin lipid raft linker 1
Rgs2	regulator of G-protein signaling 2
Rhpn2	rhophilin, Rho GTPase binding protein 2
Rnasel	ribonuclease L (2', 5'-oligoisoadenylate synthetase-dependent)
Rnf157	ring finger protein 157
Ropn1l	ropporin 1-like
Rp2h	retinitis pigmentosa 2 homolog (human)
Runx1t1	runt-related transcription factor 1; translocated to, 1 (cyclin D-related)
Scd1	stearoyl-Coenzyme A desaturase 1
Scn5a	sodium channel, voltage-gated, type V, alpha
Scrn1	secernin 1
Sema3d	sema domain, immunoglobulin domain (Ig), short basic domain, secreted, (semaphorin) 3D
Sema5a	sema domain, seven thrombospondin repeats (type 1 and type 1-like), transmembrane domain (TM) and short cytoplasmic domain, (semaphorin) 5A
Serpinb6b	serine (or cysteine) peptidase inhibitor, clade B, member 6b
Serping1	serine (or cysteine) peptidase inhibitor, clade G, member 1
Sfmbt2	Scm-like with four mbt domains 2
Sft2d2	SFT2 domain containing 2
Sh3bgr	SH3-binding domain glutamic acid-rich protein
Sigirr	single immunoglobulin and toll-interleukin 1 receptor (TIR) domain
Slc16a13	solute carrier family 16 (monocarboxylic acid transporters), member 13
Slc1a5	solute carrier family 1 (neutral amino acid transporter), member 5
Slc24a6	solute carrier family 24 (sodium/potassium/calcium exchanger), member 6
Slc25a23	solute carrier family 25 (mitochondrial carrier; phosphate carrier), member 23
Slc25a30	solute carrier family 25, member 30
Slc27a1	solute carrier family 27 (fatty acid transporter), member 1

Slc2a3	solute carrier family 2 (facilitated glucose transporter), member 3
Slc2a6	solute carrier family 2 (facilitated glucose transporter), member 6
Slc31a2	solute carrier family 31, member 2
Slc48a1	solute carrier family 48 (heme transporter), member 1
Slc7a7	solute carrier family 7 (cationic amino acid transporter, y+ system), member 7
Slc9a2	solute carrier family 9 (sodium/hydrogen exchanger), member 2
Slc9a3r1	solute carrier family 9 (sodium/hydrogen exchanger), member 3 regulator 1
Snx10	sorting nexin 10
Sord	sorbitol dehydrogenase
Spint1	serine protease inhibitor, Kunitz type 1
Spn	sialophorin
St6gal1	beta galactoside alpha 2,6 sialyltransferase 1
Stap2	signal transducing adaptor family member 2
Stard9	START domain containing 9
Stk32b	serine/threonine kinase 32B
Strbp	spermatid perinuclear RNA binding protein
Stx11	syntaxin 11
Svip	small VCP/p97-interacting protein
Sybu	syntabulin (syntaxin-interacting)
Syngr1	synaptogyrin 1
Syt11	synaptotagmin XI
Tbc1d4	TBC1 domain family, member 4
Tcf4	transcription factor 4
Tdrkh	tudor and KH domain containing protein
Tek	endothelial-specific receptor tyrosine kinase
Tgfbr1	transforming growth factor, beta receptor I
Tgm2	transglutaminase 2, C polypeptide
Thbd	thrombomodulin
Thsd4	thrombospondin, type I, domain containing 4
Tlcd1	TLC domain containing 1
Tlk1	tousled-like kinase 1
Tlr3	toll-like receptor 3
Tlr4	toll-like receptor 4
Tm7sf2	transmembrane 7 superfamily member 2
Tm7sf3	transmembrane 7 superfamily member 3
Tmem106c	transmembrane protein 106C
Tmem14a	transmembrane protein 14A
Tmem25	transmembrane protein 25
Tmem64	transmembrane protein 64
Tmem71	transmembrane protein 71
Tnfaip2	tumor necrosis factor, alpha-induced protein 2
Tnfrsf22	tumor necrosis factor receptor superfamily, member 22
Tom1l1	target of myb1-like 1 (chicken)
Tox2	TOX high mobility group box family member 2
Tpd52	tumor protein D52
Tpd52l1	tumor protein D52-like 1
Trib2	tribbles homolog 2 (Drosophila)
Trim16	tripartite motif-containing 16
Trim7	tripartite motif-containing 7
Tslp	thymic stromal lymphopoietin
Tspan11	tetraspanin 11
Tspan15	tetraspanin 15
Ttc19	tetratricopeptide repeat domain 19
Ttc21b	tetratricopeptide repeat domain 21B
Tuft1	tuftelin 1
Txnrd3	thioredoxin reductase 3
Uap1l1	UDP-N-acteylglucosamine pyrophosphorylase 1-like 1
Ube2l6	ubiquitin-conjugating enzyme E2L 6
Uchl1	ubiquitin carboxy-terminal hydrolase L1
Unc45a	unc-45 homolog A (C. elegans)
Vat1	vesicle amine transport protein 1 homolog (T californica)

Wbp2	WW domain binding protein 2
Wnt4	wingless-related MMTV integration site 4
Xdh	xanthine dehydrogenase
Xiap	X-linked inhibitor of apoptosis
Xpo7	exportin 7
Yipf2	Yip1 domain family, member 2
Ypel1	yippee-like 1 (Drosophila)
Zbtb20	zinc finger and BTB domain containing 20
Zdhhc2	zinc finger, DHHC domain containing 2
Zfp467	zinc finger protein 467
Zfp605	zinc finger protein 605
Znrf2	zinc and ring finger 2